4

Aspects of non-Markovian Open Quantum Systems

This chapter deals with non-Markovian aspects in Open Quantum Systems. The study of quantum systems interacting with the ambient environment helps in characterizing the dynamics of system and is useful in many application of quantum mechanics where system-environment interactions cannot be avoided.

4.1 Introduction

In many practical situations, the system-environment interaction brings in pronounced memory effects leading to the emergence of non-Markovian dynamics [59–63, 65, 268]. Recently, non-Markovianity has been a subject matter of various studies from quantum cryptography [66, 67], quantum biology [68–70], quantum metrology [71, 72] and quantum control [73]. It has been shown with ample evidence that non-Markovian channels can be advantageous over Markovian ones. In [74], it was reported that the non-Markovianity can enhance the channel capacity in comparison to the Markovian case. Non-Markovian behavior is a multifaceted phenomenon which can not be attributed to a unique feature of the system-environment interaction. Consequently, several different measures were introduced in order to quantify the non-Markovian behavior, viz., trace distance [59], fidelity [75], semigroup property [76] or divisibility [60] of the dynamical map, quantum Fisher information (QFI) [77], quantum mutual information [78]. In general, these measures are inequivalent and different predictions by these measures have been reported in [79].

The non-Markovian aspects become pertinent while dealing with quantum channels subjected to different types of environment. Another aspect of the system-environment interactions is the loss of the coherence and entanglement which is undesirable from the perspective of carrying out the tasks of quantum information. Therefore, this calls for the characterization of the quantum channels under the influence of different environments. Efforts have been made in this direction [80, 81]. Quantum coherence can be thought of as a resource [82–84] bringing out the utility of the quantum behavior in various tasks [85, 86]. As the system evolves under ambient conditions, modeled by the noisy channel under consideration, it has a tendency of getting mixed [87]. A pertinent question then to ask is the trade-off between the mixedness and coherence [88, 89]. The interplay between coherence and mixing in the context of non-Markovian evolution, has been studied [90]. Gate fidelity [91], which tell us about the efficiency of the gate's performance and channel fidelity [80], a measure of how well a gate preserves the distinguishability of states, and is thus connected to the Holevo bound of the channel, are two useful channel performance parameters. The performance of Lindbladian channels, such as the squeezed generalized amplitude damping (SGAD) channel [92] and the Unruh channel [93] have been studied using these parameters [80].

The rest of chapter is divided into six sections. Section 4.2, discusses various facets of quantum information under non-Markovian evolution [98]. In Sec. 4.3, LGI is studied in a two level atom interacting with a squeezed thermal bath [269]. Section 4.4 is devoted to the study of a coherence based measure of quantumness of (non) Markovian channels [107]. In Sec. 4.5, a measure of quantumness of channels based on the incompatibility of operators is proposed and studied for some well known channels, both Markovian as well as non-Markovian [108]. Section 4.9 brings out the subtitles arising in formulating the LGI for systems undergoing non-Markovian evolution [99]. In Sec. **??**, a formalism is developed for probing non-Markovian dynamics via generalized measurements [270].

4.2 Facets of quantum information under non-Markovian evolution

Here, we briefly describe various facets of quantum information studied in a qubit subjected to non-Markovian evolution, in particular, random telegraph noise (RTN) and non-Markovian dephasing (NMD) channels based on [98].

Quantum Fisher Information (QFI): Consider a d-dimensional quantum (qudit) state ρ_α depending on parameter α. The QFI [271, 272] is a measure of the information with respect to the precision of estimating the inference parameter. For the state parameter α, the Fisher information is defined as

$$F_\alpha = \frac{\left[\vec{\zeta}(\alpha) \cdot \partial_\alpha \vec{\zeta}(\alpha)\right]^2}{1 - |\vec{\zeta}(\alpha)|^2} + \left|\vec{\zeta_\alpha}(\alpha)\right|^2. \tag{4.1}$$

Here, $\vec{\zeta}(\alpha) = [\zeta_1(\alpha), \zeta_2(\alpha), \zeta_3(\alpha)]$ is the Bloch vector for the general qubit state $\rho = \frac{1}{2}\mathbf{1} + \vec{\zeta}(\alpha) \cdot \vec{\sigma}$, with $\vec{\sigma}$ denoting the Pauli spin matrix triplet $(\sigma_x, \sigma_y, \sigma_z)$. One can define the QFI-flow as the time rate of change of the QFI as

$$\mathcal{F}_\alpha = \frac{dF_\alpha}{dt}. \tag{4.2}$$

In [77], it was proposed that a positive QFI-flow at time t implies that the QFI flows back into the system from the environment, generating a non-Markovian dynamics. Therefore, we have

$$\mathcal{F}_\alpha = \begin{cases} < 0 & \text{Markovian dynamics,} \\ \\ > 0 & \text{non} - \text{Markovian dynamics.} \end{cases} \tag{4.3}$$

The back flow of QFI is linked to the divisibility property of the underlying dynamical map.

Quantum coherence: Quantum coherence is a consequence of quantum superposition and is necessary for existence of entanglement and other quantum correlations. The degree of quantum coherence in a state described by density matrix ρ is given by its off-diagonal elements. Specifically, the sum of the absolute values of the off-diagonal elements of ρ serves as a measure of the coherence

$$C = \sum_{i \neq j} |\rho_{ij}|. \tag{4.4}$$

The coherence parameter C tends to zero with increase in mixing.

Purity and Mixedness of quantum states: For a normalized state ρ, the purity is a scalar quantity $\text{Tr}\left[\rho^2\right]$ which is a measure of how much mixed a state is. Alternatively, one can define
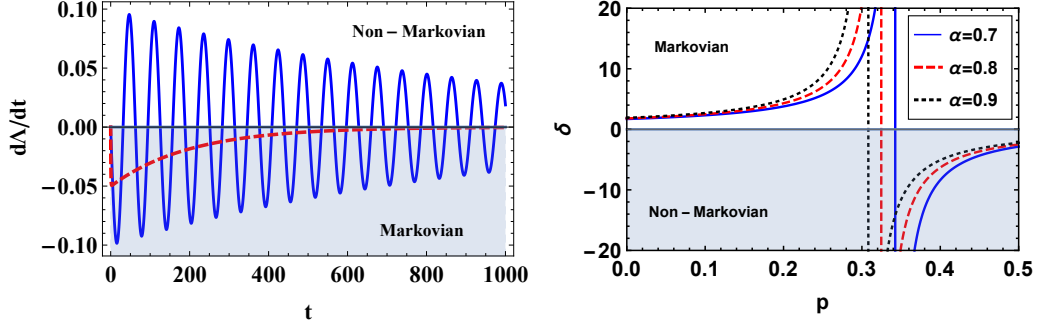
Figure 4.1: Behavior of decoherence rate with respect to time t (unit of t is *second* throughout this section) for RTN (left) and with respect to p, a dimensionless parameter, for NMD (right) channels, respectively. The non-Markovian dynamics is implied by $d\Lambda/dt > 0$ ($\delta < 0$). In case of RTN, the solid (blue) and dashed (red) curves correspond to non-Markovian ($a = 0.05, \gamma = 0.001$) and Markovian ($a = 0.05, \gamma = 1$) cases, respectively. Further, for RTN, the magnitude of the dashed (red) curve is increased ten times. The Markovian and non-Markovian regimes are separated by a singularity (vertical line) for the NMD channel.

the mixedness parameter

$$\mathcal{M} = 2\left(1 - \text{Tr}\left[\rho^2\right]\right), \tag{4.5}$$

such that $\mathcal{M} = 0$ for pure state and $\mathcal{M} = 2(1 - \frac{1}{d})$ for maximally mixed state. The interplay between coherence and mixedness was studied in [88]. For an arbitrary quantum state (ρ), in d-dimensional Hilbert space, the trade-off between coherence and mixing is quantified by the parameter β given as:

$$\beta = \frac{C^2}{(d-1)^2} + \mathcal{M} \leq 1. \tag{4.6}$$

Average gate fidelity: One of the important tasks in quantum computation and quantum information is characterization of the quantum gates and quantum channels. In this direction, the average gate fidelity is a useful tool to quantify the quality of the quantum gates and is given by the compact expression

$$G_{av} = \frac{1}{d(d+1)}\left(d + \sum_k \text{Tr}\left[E_k\right]\right). \tag{4.7}$$

Here, d is the dimension of the system and E_k are the Kraus operators characterizing the quantum channel. It gives some idea of how well a quantum gate performs an operation it is supposed to implement.

Holevo information: Given any measurement described by the positive operator valued measure (POVM) $\{E_k\}$ performed on state $\rho = \sum_i p_i \rho_i$, we define the Holevo quantity as

$$\chi_H = S(\rho) - \sum_i p_i S(\rho_i). \tag{4.8}$$

Holevo quantity represents the maximum amount of classical information that can be transmitted over a quantum channel.

We now study the above mentioned information theoretic quantities in some well known quantum channels.
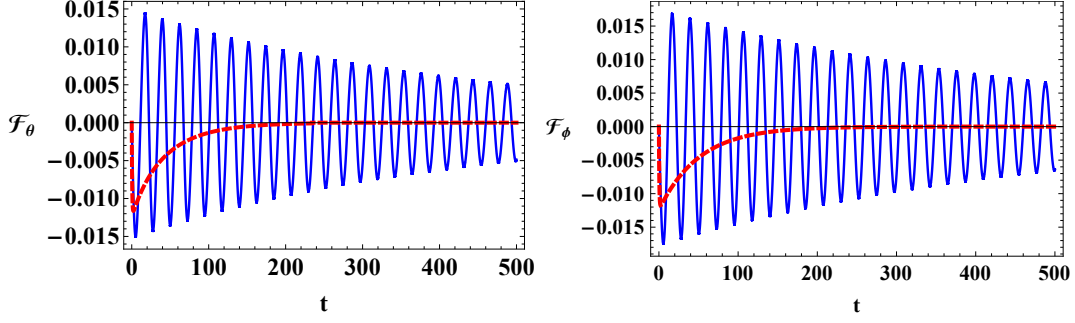
Figure 4.2: RTN noise model: Fisher information flow corresponding to the parameters θ (left) and ϕ (right), as defined in Eqs. (4.23) and (4.24), respectively, are plotted with respect to time. Solid (blue) and dashed (red) curves correspond to the non-Markovian ($a = 0.07, \gamma = 0.001$) and Markovian ($a = 0.07, \gamma = 1$) cases, respectively. The state variable θ is chosen to be $\pi/4$. The magnitude of the dashed (red) curve is increased five times.

Random Telegraph Noise: The Random Telegraph Noise (RTN) is characterized by the autocorrelation function given as

$$\langle \mathcal{X}(t)\mathcal{X}(s) \rangle = a^2 e^{-\gamma|t-s|}, \tag{4.9}$$

with $\mathcal{X}$ being the stochastic variable. The parameter a is proportional to the system environment coupling strength and γ controls the fluctuation rate of the RTN. The map, $\mathcal{E}$, governing the time evolution under RTN has the following Kraus representation

$$\mathcal{E}[\rho] = K_1 \rho K_1^\dagger + K_2 \rho K_2^\dagger, \tag{4.10}$$

with

$$K_1(\nu) = \sqrt{\frac{1 + \Lambda(\nu)}{2}}\mathbf{I}, \text{ and } K_2(\nu) = \sqrt{\frac{1 - \Lambda(\nu)}{2}}\sigma_z. \tag{4.11}$$

Here, $\Lambda(\nu) = e^{-\nu}[\cos(\nu\mu) + \frac{1}{\mu}\sin(\nu\mu)]$, with $\mu = \sqrt{(\frac{2a}{\gamma})^2 - 1}$ and $\nu = \gamma t$. The dynamics is Markovian or non-Markovian depending on whether $(\frac{2a}{\gamma})^2 > 1$ or $(\frac{2a}{\gamma})^2 < 1$, respectively.

Consider a general qubit state at time t_0 given as

$$\rho = \begin{bmatrix} \cos^2 \frac{\theta}{2} & \frac{1}{2}e^{-i\phi}\sin\theta \\ \frac{1}{2}e^{i\phi}\sin\theta & \sin^2 \frac{\theta}{2} \end{bmatrix}. \tag{4.12}$$

Under RTN noise, the state at some late time t is given by

$$
\begin{aligned}
\rho' = \mathcal{E}_{t \leftarrow t_0}[\rho] &= K_1 \rho K_1^\dagger + K_2 \rho K_2^\dagger = \frac{1 + \Lambda(t)}{2}\rho + \frac{1 - \Lambda(t)}{2}\sigma_3 \rho \sigma_3^\dagger \\
&= \begin{bmatrix} \cos^2 \frac{\theta}{2} & \frac{1}{2}e^{-i\phi}\sin\theta\Lambda(t) \\ \frac{1}{2}e^{i\phi}\sin\theta\Lambda(t) & \sin^2 \frac{\theta}{2} \end{bmatrix}.
\end{aligned}
\tag{4.13}
$$

Now, the dephasing master equation in its canonical form is given by

$$\dot{\rho} = \xi(-\rho + \sigma_z \rho \sigma_z), \tag{4.14}$$

where ξ is the decoherence rate. The necessary and sufficient condition for a map to be CP-divisible is that the decoherence rate must be non-negative [217]. Using Eqs. (4.13) and (4.14), the decoherence rate for the dephasing RTN map turns out to be

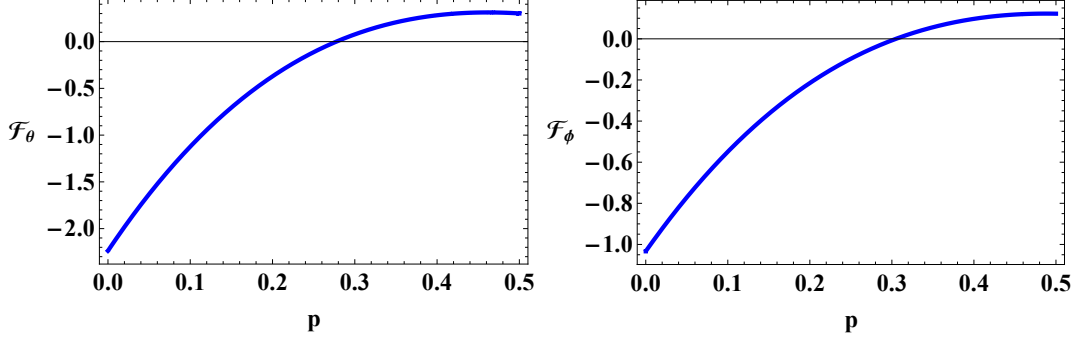$$\xi = -\frac{1}{2\Lambda}\frac{d\Lambda}{dt}. \tag{4.15}$$

44

Figure 4.3: Fisher information flow $\mathcal{F}_\alpha$ ($\alpha = \theta, \phi$), as defined in Eqs.(4.25) and (4.26), for non-Markovian dephasing dynamics. Non-Markovian dynamics is implied by $\mathcal{F}_\alpha > 0$. The parameters used are $\theta = \pi/4$ and $\alpha = 0.7$.
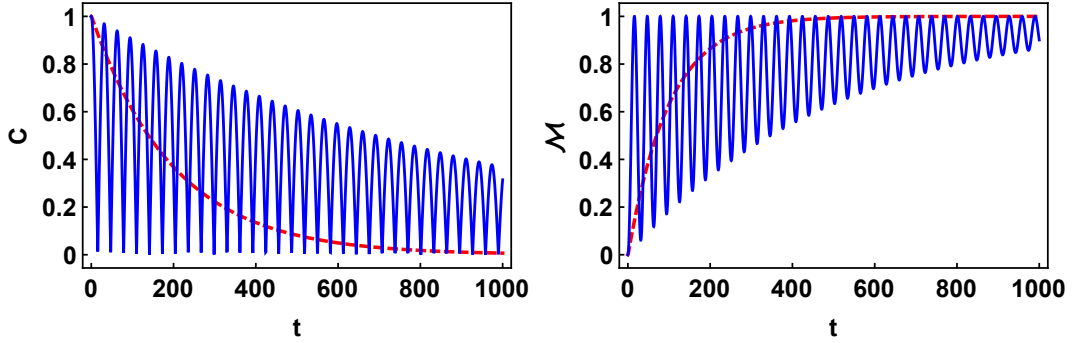

Figure 4.4: Coherence parameter C (left panel) and mixedness parameter $\mathcal{M}$ (right panel) for a qubit under RTN evolution. The solid (blue) and dashed (red) curves correspond to non-Markovian and Markovian cases, respectively. Here, we have used $\theta = \pi/2$. The values of a and γ are the same as used in Fig. 4.2.

Since $\Lambda > 0$, the decoherence rate is negative when $\frac{d\Lambda}{dt}$ is positive. The negative decoherence rate is a signature of non-Markovian dynamics. As shown in Fig. 4.1, RTN shown negative decoherence rates for certain ranges of time t. This is consistent with the non-Markovian behavior studied using the QFI-flow, detailed below.

Non-Markovianian dephasing: The non-Markovina dephasing (NMD) is governed by the following Kraus operators

$$
\begin{aligned}
K_I &= \sqrt{[1 - \alpha p](1 - p)}\ \mathbf{I} = \sqrt{1 - \kappa}\ \mathbf{I}, \\
K_z &= \sqrt{[1 + \alpha(1 - p)]p}\ \sigma_z = \sqrt{\kappa}\ \sigma_z.
\end{aligned}
\tag{4.16}
$$

Here, $0 \leq \alpha \leq 1$ and p is a monotonically increasing function of time such that $0 \leq p \leq 1/2$. The above map reduces to conventional dephasing in the limit $\alpha \to 0$. The action of the map, $\mathcal{E}^{NMD}$, given by Kraus operators in Eq. (4.16), on a general qubit state in Eq. (4.12) is

$$
\rho' = \mathcal{E}^{NMD}_{t \leftarrow t_0}[\rho] = \begin{bmatrix} \cos^2 \frac{\theta}{2} & \frac{1}{2} e^{-i\phi} \sin(\theta)\Omega \\ \frac{1}{2} e^{i\phi} \sin(\theta)\Omega & \sin^2 \frac{\theta}{2} \end{bmatrix}.
\tag{4.17}
$$

Here, $\Omega = 1 - 2p + 2p\alpha(p - 1) = 1 - 2\kappa$. Corresponding to the Kraus operators in Eq. (4.16), the canonical master equation is

$$
\dot{\rho} = \delta(-\rho + \sigma_z \rho \sigma_z).
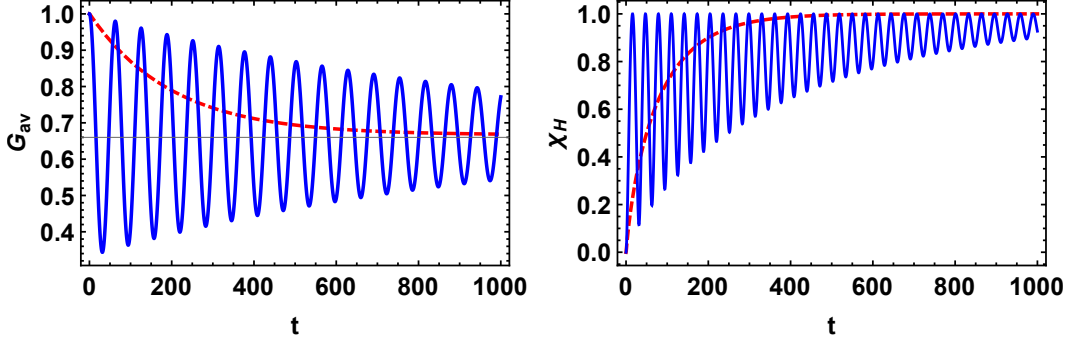\tag{4.18}
$$

Figure 4.5: Average gate fedility G_{av} parameter (left) and Holevo quantity χ_H (right) in RTN case. The solid (blue) and dashed (red) curves correspond to non-Markovian and Markovian cases, respectively. The parameters a and γ are as given in Fig. 4.2. The state parameter $\theta = \pi/2$.

Here, $\dot{\rho} = \frac{d\rho}{dp}$ and the decoherence rate $\delta = \delta(p)$ as well as the state $\rho = \rho(p)$ are functions of the parameter p. Using Eqs. (4.17) and (4.18), the decoherence rate turns out to be

$$\delta = \frac{\frac{1}{2}(r_+ + r_-) - p}{(p - r_-)(p - r_+)}, \tag{4.19}$$

with $r_\pm = (1 + \alpha \pm \sqrt{1 + \alpha^2})/2\alpha$. The regimes $p < r_-$ and $p > r_-$ correspond to Markovian and non-Markovian dynamics, respectively. The behavior of δ as a function of parameter p is shown in Fig. 4.1. The singularity occurs at $p = r_-$, which, in turn, depends on the value of parameter α.

Table 4.1: Analytic expressions for various quantities studied in RTN and NMD models.

Facets ↓ Models→	RTN	NMD
Coherence (C)	$\left\|\Lambda \sin\theta\right\|$	$\left\|(1 - 2\kappa)\sin(\theta)\right\|$
Mixedness ($\mathcal{M}$)	$(1 - \Lambda^2)\sin^2\theta$	$(1 - (1 - 2\kappa)^2)\sin^2\theta$
Coherence-Mixing balance (β)	$\sin^2\theta$	$\sin^2\theta$
Average gate fidelity	$(1 + \|1 + \Lambda\|)/3$	$(1 + \|1 + (1 - 2\kappa)\|)/3$
Holevo information	$-\lambda_+ \mathrm{Log}_2\lambda_+ - \lambda_-\mathrm{Log}_2\lambda_-$	$\frac{4p(1-3\alpha(p-1))\tanh^{-1}(X)-3\ln\left(2\alpha(p-1)p-\frac{2p}{3}+1\right)}{\ln(8)}$

Here $\lambda_\pm = \frac{1}{4}\left(2 \pm \sqrt{2}\sqrt{1 + \Lambda^2 + (1 - \Lambda^2+)\cos 2\theta}\right)$, $\Lambda = e^{-\nu}[\cos(\nu\mu) + \frac{1}{\mu}\sin(\nu\mu)]$, $\kappa = p[1 + \alpha(1 - p)]$, and $X = 4\alpha(p - 1)p - \frac{4p}{3} + 1$. Also, θ is the state parameter, Eq. (4.12).

4.2.1 Quantum Fisher infomation flow and non-Markovianity

In this section, we discuss the interplay between QFI-flow and non-Markovianity in the context of RTN and NMD channels by using the dynamics sketched in the previous section.

For RTN channel: We will use the time evolved state given in Eq. (4.13) and compute the QFI and QFI-flow. The Bloch vector corresponding to ρ' in Eq. (4.13) turns out to be

$$\vec{\zeta}(\theta, \phi) = \left(\frac{1}{2}\Lambda(\nu)\sin\theta\cos\phi, \frac{1}{2}\Lambda(\nu)\sin\theta\sin\phi, \frac{1}{2}\cos\theta\right). \tag{4.20}$$

Therefore,

$$\partial_\theta \vec{\zeta}(\theta, \phi) = \left(\frac{1}{2}\Lambda(\nu)\cos\theta\cos\phi, \frac{1}{2}\Lambda(\nu)\cos\theta\sin\phi, -\frac{1}{2}\sin\theta\right),$$

$$\partial_\phi \vec{\zeta}(\theta, \phi) = \left(-\frac{1}{2}\Lambda(\nu)\sin\theta\sin\phi, \frac{1}{2}\Lambda(\nu)\sin\theta\cos\phi, 0\right).$$

Also,

$$\vec{\zeta}(\theta, \phi) \cdot \partial_\phi \vec{\zeta}(\theta, \phi) = 0,$$

$$\vec{\zeta}(\theta, \phi) \cdot \partial_\theta \vec{\zeta}(\theta, \phi) = \frac{1}{4}((\Lambda(\nu))^2 - 1)\sin\theta\cos\theta,$$

$$|\vec{\zeta}(\theta, \phi)|^2 = \frac{1}{4}(\Lambda(\nu))^2 \sin^2(\theta) + \frac{1}{4}\cos^2\theta. \tag{4.21}$$

With above setting, the QFI corresponding to the parameters θ and ϕ becomes

$$F_\theta = 1 + \frac{3(-4 + \Lambda^2)}{2(7 - \Lambda^2 + (-1 + \Lambda^2)\cos 2\theta)},$$

$$F_\phi = \frac{1}{4}\Lambda^2 \sin^2\theta. \tag{4.22}$$

The corresponding QFI-flows are given by the following expressions

$$\mathcal{F}_\theta = \frac{dF_\theta}{dt} = -\frac{18\gamma\mu^2\left(\mu^2 + 1\right)\cos^2(\theta)e^{2\gamma t}\sin(\gamma\mu t)\mu\Lambda(t)}{\left[\mu^2(\cos(2\theta) - 7)e^{2\gamma t} + 2\sin^2(\theta)\mu^2\Lambda^2(t)\right]^2}, \tag{4.23}$$

$$\mathcal{F}_\phi = \frac{dF_\phi}{dt} = \frac{1}{2}\sin^2\theta\frac{d\Lambda}{dt} = \frac{\gamma\left(\mu^2 + 1\right)\sin^2(\theta)e^{-2\gamma t}\sin^2(\gamma\mu t)(\mu\cot(\gamma\mu t) + 1)}{2\mu^2}. \tag{4.24}$$

These quantities are depicted in the Fig. 4.2 both for the Markovian as well as the non-Markvoian cases.

For NMD channel: The analytic expressions for the QFI-flow in this case are given as

$$\mathcal{F}_\theta = \frac{9\cos^2(\theta)(2\alpha(p-1)p - 2p + 1)(\alpha(2p-1) - 1)}{(2(p-1)p\cos(2\theta)(\alpha(p-1) - 1)(\alpha p - 1) - 2(p-1)p(\alpha(p-1) - 1)(\alpha p - 1) + 3)^2}, \tag{4.25}$$

$$\mathcal{F}_\phi = \sin^2(\theta)(2\alpha(p-1)p - 2p + 1)(\alpha(2p-1) - 1). \tag{4.26}$$

These quantities are plotted in Fig. 4.3. The various facets studied in RTN and NMD models are listed in Table (4.1) with their compact analytic expressions.

4.2.2 Results and discussion

The nature of the dynamics is governed by the decoherence rate, which is positive (negative) for Markovian (non-Markovian) dynamics. In the specific models considered in this work, namely RTN and NMD, the behavior of the respective decoherence rates is depicted in Fig. 4.1. This behavior is in concord with that seen with the QFI-flow. The non-Markovian behavior in case of RTN is controlled by the channel parameters, while the NMD is non-Markoviann for all values of the parameter α. Figure 4.2 depicts the QFI-flow corresponding to the state parameters θ and
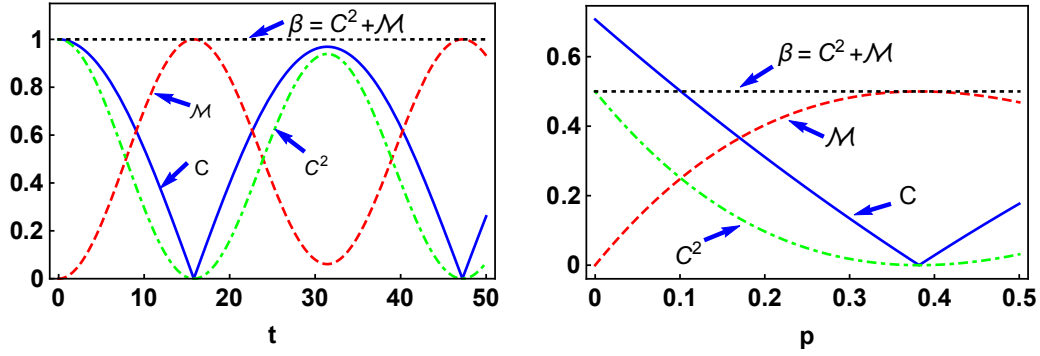
Figure 4.6: Interplay between coherence (C) and mixedness ($\mathcal{M}$) quantified by the parameter $\beta = C^2 + \mathcal{M}$, Eq. (4.6). Left and right panel corresponds to RTN and NMD cases, respectively. For RTN, $a = 0.5$, $\gamma = 0.001$ (non-Markovian case, similar trade-off is observed in Markovian case, not displayed here) and $\theta = \pi/2$, while for NMD the channel, $\alpha = 0.5$ and $\theta = \pi/4$.
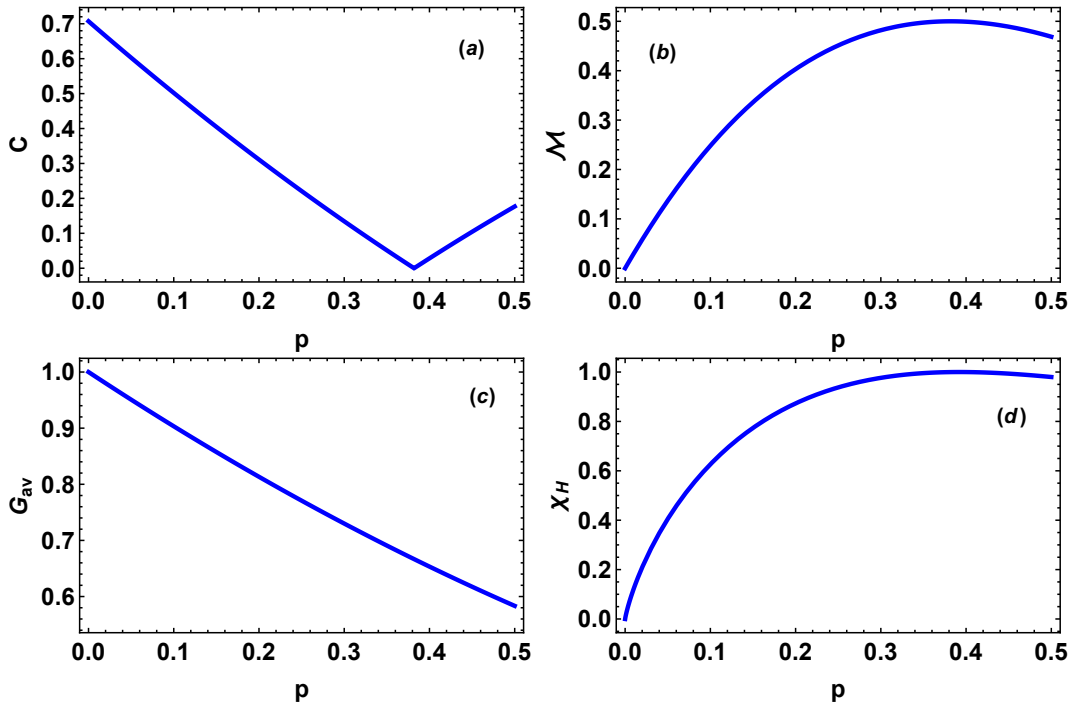

Figure 4.7: Non-Markovina Dephasing (NMD) channel. Showing (a) coherence parameter (b) mixedness parameter (c) average gate fidelity and (d) Holevo quantity. The state parameters used are $\theta = \pi/4$ and $\phi = 0$, and the channel parameter $\alpha = 0.5$.

ϕ as a function of time. The positive QFI-flow is a signature of non-Markovianity and is linked with the divisibility of the underlying dynamical map. It is well known that the non-Markovianity emerges in the RTN governed dynamics under the condition $2a > \gamma$. In this regime, QFI-flow is found to oscillate symmetrically about zero, thereby confirming the non-Markovian nature of the dynamics. The behavior of the coherence and mixedness under RTN evolution is shown in Fig. 4.4. The coherence parameter C and the mixedness parameter $\mathcal{M}$ decrease (increase) monotonically in the Markovian regime unlike the non-Markovian case. In the non-Markovian regime, these parameters shown recurrent behavior with time with an envelope of damped oscillation. The interplay between coherence and mixedness is symmetric in RTN model, Fig. 4.6, such that the increase in one is accompanied with the decrease in other. The parameter β, Eq. (4.6), depends only on the state parameter θ, as given in Table (4.1). Similar observations are made for the average gate fidelity (G_{av}) and Holevo quantity and are depicted in Fig. 4.5 where the monotonic decrease with respect to time in Markovian case is contrasted with the oscillating behavior of these quantities in the non-Markovian scenario.

The decoherence rate in non-Markovian dephasing (NMD) model shows a negative branch separated from the positive branch by a singularity. However, the recurrent behavior observed in RTN is missing. The QIF-flow is positive for certain range of the time like parameter p, as depicted in Fig. 4.3, demonstrating the non-Markovian nature of this model. The complementary behavior of coherence and mixedness is observed, that is, the decrease in the coherence is accompanied by an increase in the mixedness, Fig. 4.6, such that the β parameter, defined in Eq. (4.6), is a function of the state variable θ, see Table (4.1). The average gate fidelity decreases, while the Holevo quantity shows an increase with p in the range $0 \leq p \leq 1/2$.

4.3 Violation of Leggett-Garg type inequalities in a driven two level atom interacting with a squeezed thermal reservoir

In this section, which is based on [269], we discuss the violation of Leggett-Garg type inequalities (LGtIs) in a two level atom, driven by an external field in the presence of a squeezed thermal reservoir. The violations are observed in the underdamped regime where the spontaneous transition rate is much smaller compared to the Rabi frequency. Increase in thermal effects is found to decrease the extent of violation as well as the time over which the violation lasts. With increase in the value of squeezing parameter the extent of violation of LGtIs is seen to reduce. The violation of LGtIs is favored by increase in the driving frequency. Further, the interplay of the degree of violation and strength of the measurements is studied. It is found that the maximum violation occurs for ideal projective measurements.

Here, we study the stationarity form of LGI as defined in Eq. (2.25) with

$$C(t_i, t_j) = \sum_{m,n=\pm} mn \, \mathrm{Tr} \left[\Pi^m \mathcal{E}_{t_j \leftarrow t_i} \left[\Pi^n \rho(t_i) \Pi^n \right] \right]. \tag{4.27}$$

The map $\mathcal{E}_{t_b \leftarrow t_a}$ governs the time evolution of the state, i.e., $\rho(t_b) = \mathcal{E}_{t_b \leftarrow t_a}[\rho(t_a)]$. Assuming that the measurements are made at time $t_2 > t_1 > t_0$, we have

$$K_\pm = \pm 2C(t_0, t) - C(t_0, 2t) \leq 1. \tag{4.28}$$

Here, $t = t_2 - t_1 = t_1 - t_0$, is the time between two successive measurements. From here on, we will call $K_\pm$ as LG parameter. Though the assumption of stationarity helps to put the inequalities into easily testable forms, it reduces the class of macrorealist theories which are put to the test

[38]. The stationarity condition holds provided the system can be prepared in a well-defined state and the system evolves under Markovian dynamics. These conditions are satisfied in the model considered in this work. Therefore, for a suitable experimental setup, inequalities (4.28) provide a tool to quantitatively probe the coherence effects in this system.

Here we study the violation of LGtIs in a driven two-level atom interacting with a squeezed thermal reservoir. Such studies are motivated by the fact that LGtIs provide a way to probe the degree of coherence in a system. Interestingly, the two time correlation functions can be written in terms of experimentally observable quantities. In recent times, the studies of LGtIs has increased considerably leading, for example, to the possible applications of LGtIs violation for ensuring security in quantum key distribution schemes. Further, LGtIs also serve to probe the applicability of the models of unsharp measurements pertaining to non-ideal measurement set ups [273]. These studies become even more pertinent from a practical perspective when one takes into account open system effects. Thus, for example, the effect of temperature, squeezing and driving frequencies, as well as the role of the strength of measurement on LGtI violation in a paradigm model of quantum optics, as done here, should pave the way for developing our understanding of the multifaceted role of various parameters on the inherent quantumness of the system, thereby helping in *characterizing* the quantumness. This would be particularly relevant from the point of view of applying such systems towards quantum technologies.

4.3.1 Model: A driven two level system

Here, we sketch the essential details of a driven two-level system in contact with a squeezed thermal bath [57, 58, 80, 92, 113]. The model consists of a two level system whose Hilbert space is spanned by two states, the ground state $|g\rangle$ and the excited state $|e\rangle$, Fig. 4.8. The description of such a system is analogous to that of a spin -$\frac{1}{2}$ system. The Pauli operators in terms of these basis vectors are $\sigma_1 = |e\rangle\langle g| + |g\rangle\langle e|$, $\sigma_2 = -i|e\rangle\langle g| + i|g\rangle\langle e|$ and $\sigma_3 = |e\rangle\langle e| - |g\rangle\langle g|$, and satisfy the usual commutation $[\sigma_i, \sigma_j] = 2i\epsilon_{ijk}\sigma_k$ and the anticommutation $\{\sigma_i, \sigma_j\} = 2\delta_{ij}$. The raising and lowering operators can be defined as

$$\sigma_+ = |e\rangle\langle g| = \frac{1}{2}(\sigma_1 + i\sigma_2), \qquad \sigma_- = |g\rangle\langle e| = \frac{1}{2}(\sigma_1 - i\sigma_2). \qquad (4.29)$$

With this setting, we can define the system Hamiltonian H_S to be diagonal in basis $\{|e\rangle, |g\rangle\}$. With ω_0 denoting the transition frequency between the two levels (setting $\hbar = 1$), we have

$$H_S = \frac{1}{2}\omega_0\sigma_3. \qquad (4.30)$$

A detailed account of two level systems and their application can be found in [274].

We now consider the case when a two level atomic transition $|e\rangle \leftrightarrow |g\rangle$ is driven by an external source. The source is assumed to be a coherent single mode field on resonance. Under dipole approximation, the Hamiltonian (in the interaction picture) is given by $H_L = -\vec{E}_L(t).\vec{D}(t)$. Here, $\vec{E}_L(t) = \vec{\epsilon}e^{-i\omega_0 t} + \vec{\epsilon}^* e^{+i\omega_0 t}$ is the electric field strength of the driving mode. Also, $\vec{D}(t) = \vec{d}\sigma_- e^{-i\omega_0 t} + \vec{d}^* \sigma_+ e^{+i\omega_0 t}$ is the atomic dipole operator in the interaction picture and $\vec{d} = \langle g|\vec{D}|e\rangle$ is the transition matrix element of the dipole operator. The atom-field interaction can be written in the rotating wave approximation as follows,

$$H_L = -\frac{\Omega}{2}(\sigma_+ + \sigma_-). \qquad (4.31)$$

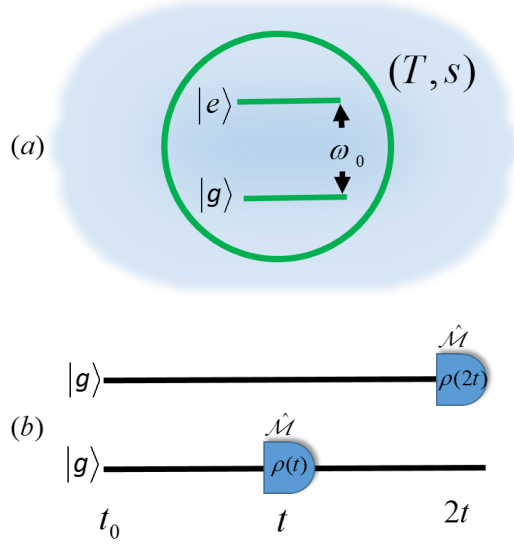Here, $\Omega = 2\vec{\epsilon}.\vec{d}^*$, is referred to as the Rabi frequency. Now coupling the system to a thermal

Figure 4.8: Schematic diagram for (a) Two level atom interacting with a squeezed thermal bath at temperature T with squeezing parameter s. The transition frequency between the two levels is ω_0. (b) Testing the LGtIs using the statistics of two experiments, with the same preparation state, $|g\rangle$, at time $t_0 = 0$. The dichotomic observable $\hat{\mathcal{M}} = |g\rangle\langle g| - |e\rangle\langle e|$ would lead to $+1$ if the atom is found in ground state and -1 otherwise. For example, at t_0, we have $\langle\hat{\mathcal{M}}\rangle = +1$.

reservoir leads to the quantum master equation

$$
\begin{aligned}
\frac{d\rho(t)}{dt} &= \frac{i\Omega}{2}\big[\sigma_+ + \sigma_-, \rho(t)\big] \\
&\quad + \gamma_0 n\left(\sigma_+\rho(t)\sigma_- - \frac{1}{2}\sigma_-\sigma_+\rho(t) - \frac{1}{2}\rho(t)\sigma_-\sigma_+\right) \\
&\quad + \gamma_0(n+1)\left(\sigma_-\rho(t)\sigma_+ - \frac{1}{2}\sigma_+\sigma_-\rho(t) - \frac{1}{2}\rho(t)\sigma_+\sigma_-\right) \\
&\quad - \gamma_0 M\sigma_+\rho(t)\sigma_+ - \gamma_0 M^*\sigma_-\rho(t)\sigma_-.
\end{aligned}
\tag{4.32}
$$

Here, $\gamma = \gamma_0(2n+1)$ is the total transition rate with γ_0 being the spontaneous emission rate. Further,

$$
\begin{aligned}
n &= n_{th}(\cosh^2(s) + \sinh^2(s)) + \sinh^2(s), \\
\text{and } M &= -\cosh(s)\sinh(s)e^{i\theta}(2n_{th}+1).
\end{aligned}
\tag{4.33}
$$

where s and θ are the squeezing parameters and $n_{th} = 1/(\exp[\beta\omega_0] - 1)$ is the Plank distribution at transition frequency. In what follows, we will set $\theta = 0$ for the purpose of calculations.

In order to solve Eq. (4.32), we write the density matrix as

$$
\rho(t) = \frac{1}{2}(\mathbf{I} + \vec{v}(t).\vec{\sigma}) = \begin{pmatrix} \frac{1}{2}(1 + \langle\sigma_3\rangle) & \langle\sigma_-\rangle \\ \langle\sigma_+\rangle & \frac{1}{2}(1 - \langle\sigma_3\rangle) \end{pmatrix},
\tag{4.34}
$$

with $\vec{v}(t) = \langle\vec{\sigma}(t)\rangle = \mathrm{Tr}[\vec{\sigma}\rho(t)]$, is known as the Bloch vector. With this notation, the master equation, Eq. (4.32), becomes

$$
\frac{d}{dt}\langle\vec{\sigma}(t)\rangle = \mathcal{G}\langle\vec{\sigma}(t)\rangle + \vec{m}.
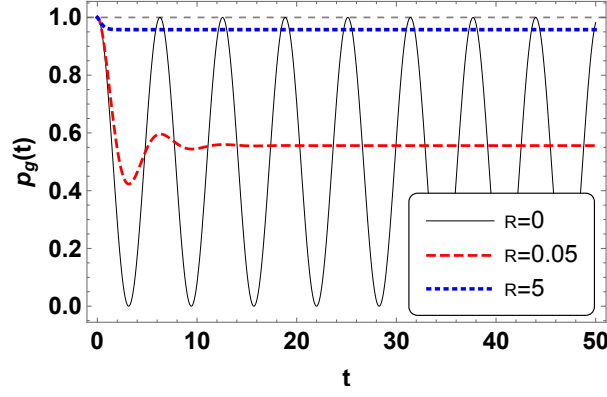\tag{4.35}
$$

Figure 4.9: Probability of finding the atom in ground state at time t, in the units with $\hbar = k_B = 1$. Here, $R = \gamma_0/\Omega$ is the ratio of the spontaneous emission to the Rabi frequency. With squeezing parameter $s = 0$ and transition frequency $\omega_0 = 0.5$, the values $R = 0$, 0.05 and 5 correspond to $\mu_s = 1$, 0.9 (underdamped) and $0.7i$ (overdamped), respectively.
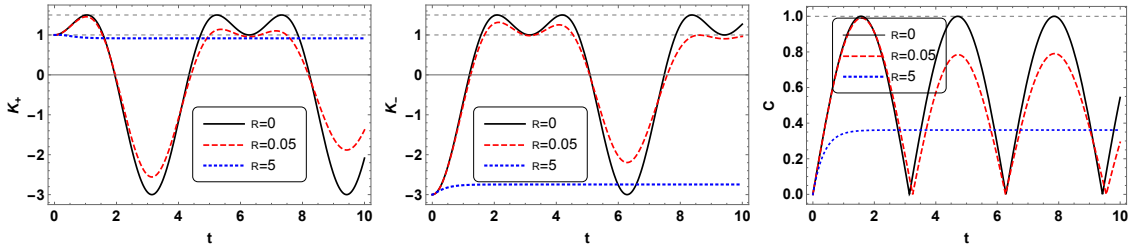

Figure 4.10: Evolution of the LG parameters K_+ (left), K_- (middle) and coherence parameter C (right). Here, $\beta = 10$, $\omega_0 = 0.5$, $s = 0$, such that $R = 0$, 0.05 and 5 correspond to $\mu_s = 1$, 0.9 (underdamped) and $0.7i$ (overdamped) cases, respectively. The violation of LGtIs occur predominantly in underdamped regime such that $K_\pm$ reach their quantum bound $3/2$ as $R \to 0$. The coherence parameter shows exponentially damped oscillations in underdamped regime, while in overdamped case, it monotonically saturates to it stationary value.

Here,

$$
\mathcal{G} = \begin{pmatrix} -\frac{\gamma}{2} - \gamma_0 M & 0 & 0 \\ 0 & -\frac{\gamma}{2} + \gamma_0 M & \Omega \\ 0 & -\Omega & -\gamma \end{pmatrix}, \tag{4.36}
$$

and $\vec{m} = [0 \ 0 \ -\gamma_0]^T$, T being the transpose operation.

The differential equation (4.35) has the stationary solution given by

$$
\langle \sigma_3 \rangle_s = -\frac{\gamma_0(\gamma - 2\gamma_0 M)}{\gamma^2 - 2\gamma\gamma_0 M + 2\Omega^2},
$$
$$
\langle \sigma_+ \rangle_s = -\frac{i\gamma_0\Omega}{\gamma^2 - 2\gamma\gamma_0 M + 2\Omega^2}. \tag{4.37}
$$

Consequently, the stationary population of the excited state $p_e^s = \frac{1}{2}(1 + \langle \sigma_3 \rangle_s) = \frac{1}{2}\Big[1 - \frac{\gamma_0(\gamma - 2\gamma_0 M)}{\gamma^2 - 2\gamma\gamma_0 M + 2\Omega^2}\Big]$.

In the strong driving limit, $\Omega \gg \gamma_s$, we have $p_e^s = 1/2$ and $\langle \sigma_+ \rangle_s = -i\gamma_0/2\Omega$.

In order to solve the time dependent Bloch equation, Eq. (4.35), it is convenient to introduce the vector

$$\langle \vec{\Sigma}(t) \rangle = \langle \vec{\sigma}(t) \rangle - \langle \vec{\sigma} \rangle_s. \tag{4.38}$$

This vector satisfies the homogeneous equation

$$\frac{d}{dt} \langle \vec{\Sigma}(t) \rangle = \mathcal{G} \langle \vec{\Sigma}(t) \rangle. \tag{4.39}$$

This equation can be easily solved by diagonalizing $\mathcal{G}$, which has the eigenvalues

$$\lambda_1 = -\frac{\gamma}{2} - \gamma_0 M,$$
$$\lambda_{2,3} = \frac{\gamma_0 M}{2} - \frac{3\gamma}{4} \pm i\mu_s, \tag{4.40}$$

where,

$$\mu_s = \sqrt{\Omega^2 - \left(\frac{\gamma_s}{4}\right)^2} \quad \text{with} \quad \gamma_s = \gamma + 2\gamma_0 M. \tag{4.41}$$

Assuming the atom to be initially in the ground state $\rho(0) = |g\rangle \langle g|$, we have

$$\langle \sigma_3(0) \rangle = -1 \quad \text{or} \quad \langle \Sigma_3(0) \rangle = -1 - \langle \sigma_3 \rangle_s, \tag{4.42}$$

and

$$\langle \sigma_\pm(0) \rangle = 0 \quad \text{or} \quad \langle \Sigma_\pm(0) \rangle = -\langle \sigma_\pm \rangle_s. \tag{4.43}$$

With these initial conditions, the solution of Eq. (4.39) is given by

$$\langle \vec{\Sigma}(t) \rangle = \begin{pmatrix} e^{-(\gamma+2\gamma_0 M)t/2} \langle \Sigma_1(0) \rangle \\ e^{(-3\gamma+2\gamma_0 M)t/4} \left[\left(\cos(\mu_s t) + \frac{\gamma+3\gamma_0 M}{4\mu_s} \sin(\mu_s t) \right) \langle \Sigma_2(0) \rangle + \frac{\Omega}{\mu_s} \sin(\mu_s t) \langle \Sigma_3(0) \rangle \right] \\ e^{(-3\gamma+2\gamma_0 M)t/4} \left[\left(1 - \frac{\gamma_0 M}{2\mu_s} \right) \cos(\mu_s t) - \frac{\gamma}{4\mu_s} \sin(\mu_s t) \right] \langle \Sigma_3(0) \rangle + \frac{i\Omega}{\mu_s} e^{(-3\gamma+2\gamma_0 M)t/4} \sin(\mu_s t) [\langle \Sigma_+(0) \rangle - \langle \Sigma_-(0) \rangle] \end{pmatrix}. \tag{4.44}$$

Having obtained the solution, one can calculate the survival probability of the atom being in the ground state $|g\rangle$, as

$$p_g(t) = \frac{1 - [\langle \Sigma_3(t) \rangle + \langle \sigma_3 \rangle_s]}{2}. \tag{4.45}$$

Further, the degree of coherence is proportional to the off-diagonal element

$$\langle \sigma_+(t) \rangle = \frac{\langle \sigma_1(t) \rangle + i\langle \sigma_2(t) \rangle}{2} + \langle \sigma_+ \rangle_s. \tag{4.46}$$

The dynamics is underdamped or overdamped depending on whether μ_s, defined in Eq. (4.41), is real or imaginary. As a result, in underdamped regime, the probabilities as well as the coherence exhibit exponentially damped oscillations, while in the over damped case, they monotonically approach their stationary values, Fig. 4.9. Throughout this work, we adopt the units $\hbar = k_B = 1$.

4.3.2 Leggett-Garg type inequality for the two level driven system

Let $\mathcal{E}_{t_j \leftarrow t_i}$ be the map corresponding to the evolution given by Eq. (4.32), such that the system in state $\rho(t_i)$ at time t_i evolves to state $\rho(t_j)$ at some later time $t_j > t_i$

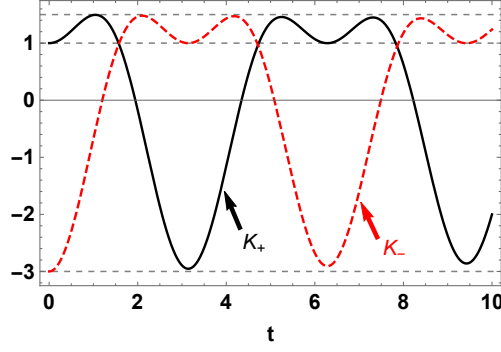$$\rho(t_j) = \mathcal{E}_{t_j \leftarrow t_i}[\rho(t_i)]. \tag{4.47}$$

Figure 4.11: Complementary behavior of LG parameters $K_\pm$ in the strong driving limit. The various parameters used are $\beta = 10$, $\omega_0 = 0.5$, $s = 0$, $R = 0.005$, pertaining to the underdamped regime.

Let at time t_0 the system be in the ground state $|g\rangle$. We define the dichotomic observable $\hat{\mathcal{M}} = |g\rangle\langle g| - |e\rangle\langle e|$. Thus a measurement of this observable leads to $+1$ or -1 depending to whether the system is in the ground or excited state, respectively, Fig. 4.8. We introduce the projectors $\Pi^+ = |g\rangle\langle g|$ and $\Pi^- = |e\rangle\langle e|$, such that $O = \Pi^+ - \Pi^-$. Using Eq. (4.27), with the notation $t_1 - t_0 = t$, the two time correlation $C(t_0, t_1)$ is

$$
\begin{aligned}
C(t_0, t_1) &= \text{Tr}[\Pi^+ \rho(t_0)] \, \text{Tr}\left[\Pi^+ \mathcal{E}_{t_1 \leftarrow t_0}\Big[\frac{\Pi^+ \rho(t_0)\Pi^+}{\text{Tr}[\Pi^+ \rho(t_0)]}\Big]\right] \\
&\quad - \text{Tr}[\Pi^+ \rho(t_0)] \, \text{Tr}\left[\Pi^- \mathcal{E}_{t_1 \leftarrow t_0}\Big[\frac{\Pi^+ \rho(t_0)\Pi^+}{\text{Tr}[\Pi^+ \rho(t_0)]}\Big]\right] \\
&\quad - \text{Tr}[\Pi^- \rho(t_0)] \, \text{Tr}\left[\Pi^+ \mathcal{E}_{t_1 \leftarrow t_0}\Big[\frac{\Pi^- \rho(t_0)\Pi^-}{\text{Tr}[\Pi^- \rho(t_0)]}\Big]\right] \\
&\quad + \text{Tr}[\Pi^- \rho(t_0)] \, \text{Tr}\left[\Pi^- \mathcal{E}_{t_1 \leftarrow t_0}\Big[\frac{\Pi^- \rho(t_0)\Pi^-}{\text{Tr}[\Pi^- \rho(t_0)]}\Big]\right], \\
&= p_g(t) - p_e(t) = 2p_g(t) - 1. \tag{4.48}
\end{aligned}
$$

Plugging in the expressions of probabilities, we have

$$
K_\pm = \pm 2\mathcal{F}(t) - \mathcal{F}(2t) \mp 1. \tag{4.49}
$$

Here,

$$
\mathcal{F}(t) = \mathcal{A}\big[\mathcal{B} + \mathcal{C}e^{-(3\gamma - 2\gamma_0 M)t/4}\cos(\mu_s t) + \mathcal{D}\sin(\mu_s t)\big] - 1, \tag{4.50}
$$

with coefficients given by

$$
\begin{aligned}
\mathcal{A} &= \big[4\mu_s(\gamma^2 - 2\gamma\gamma_0 M + 2\Omega^2)\big]^{-1}, \\
\mathcal{B} &= 4(\gamma + \gamma_0)(\gamma - 2\gamma_0 M)\mu_s + 8\mu_s\Omega^2, \\
\mathcal{C} &= -2(\gamma_0 M - 2\mu_s)\big[(\gamma - \gamma_0)(\gamma - 2\gamma_0 M) + 2\Omega^2\big], \\
\mathcal{D} &= -\gamma(\gamma - \gamma_0)(\gamma - 2\gamma_0 M) - 2(\gamma - 4\gamma_0)\Omega^2. \tag{4.51}
\end{aligned}
$$

In the strong driving limit, $\Omega \gg \gamma_s$, the coefficients can be approximated as $\mathcal{A} \approx \Omega^{-3}$, $\mathcal{B} \approx \mathcal{C} \approx \Omega^3$ and $\mathcal{D} \approx \Omega^2$, such that in this limit, $\mathcal{F}(t) \propto \cos(\Omega t)$ and therefore

$$
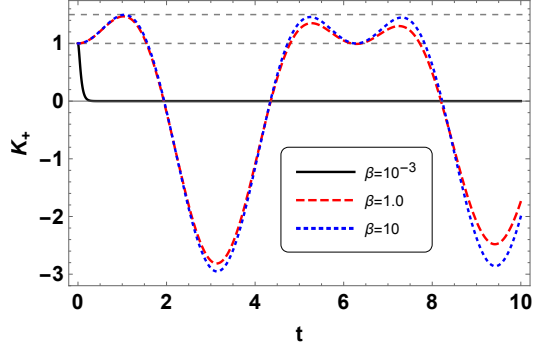K_\pm \approx \pm 2\cos(\Omega t) - \cos(2\Omega t). \tag{4.52}
$$

Figure 4.12: Temperature dependence of LG parameter K_+. With $\omega_0 = 0.5$, $s = 0$ and $R = 0.005$, the values $\beta = 10$, 1 and 10^{-3} correspond to $\mu_s = 1$, 0.9 (underdamped) and $4.8i$ (overdamped), respectively.

Effect of weak measurement: The two time correlation function $C(t_0, t)$, Eq. (4.48), was obtained by assuming that the measurements are ideal or projective. However, it would be interesting to see how weak measurements affect the behavior of $C(t_0, t)$ and thereby of the LG parameters $K_\pm$. The weak measurements are characterized by invoking a parameter ξ [275, 276], such that the ideal projectors $\Pi^\pm$ are replaced by the "weak projectors" $W^\pm$ defined as

$$W^\pm = \left(\frac{1 \pm \xi}{2}\right)\Pi^+ + \left(\frac{1 \mp \xi}{2}\right)\Pi^-.$$

(4.53)

Here, $0 < \xi \le 1$, such that when $\xi = 1$, $W^\pm$ reduce to the ideal projection operators $\Pi^\pm$. Invoking weak projectors leads to the following form of the two time correlation function $C(t_0, t)|_{weak} = \xi^2 C(t_0, t)$, and consequently

$$K_\pm|_{weak} = \xi^2 K_\pm.$$

(4.54)

Therefore, the maximum violation of LGtI occurs for an ideal projective measurement.

4.3.3 Results and discussion

The LGtIs given by inequality (4.28) are studied in the context of a two level atom with the ground and excited states labelled as $|g\rangle$ and $|e\rangle$, respectively. An external field is driving the transition between the two levels. Further, the atom is allowed to interact with a squeezed thermal bath. The inequalities thus obtained are in terms of experimentally relevant parameters. The violation of LGtIs occur predominantly in the underdamped regime which is characterized by the real values of parameter μ_s defined in Eq. (4.41), such that

$$\Omega > \frac{\gamma_s}{4} = \gamma_0 \frac{(2n+1) + 2M}{4} \quad \text{underdamped,}$$
$$\Omega < \frac{\gamma_s}{4} = \gamma_0 \frac{(2n+1) + 2M}{4} \quad \text{overdamped.}$$

(4.55)

Here, the parameter $\gamma_s = \gamma_0[(2n+1) + 2M]$, as defined in Eq. (4.41). Figure 4.10 depicts the behavior of LG parameters $K_\pm$ with respect to time t, for different values of the ratio $R = \gamma_0/\Omega$. The violations of LGtIs are observed mainly in the underdamped regime and fade quickly with the increase in R. In other words, strong driving favors the violation of LGtIs to their maximum quantum bound. The right most panel of the figure shows coherence paramter C [8, 90] which is defined as

$$C = \sum_{i \neq j} |\rho_{ij}|.$$

(4.56)

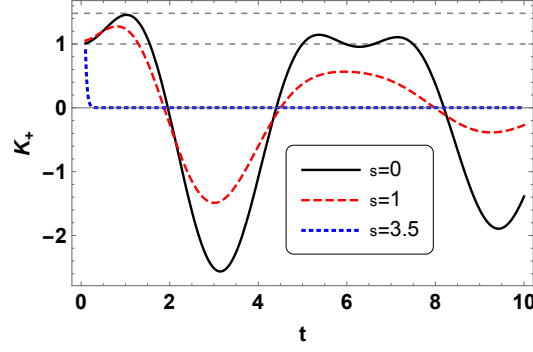The extent of violation of LGtIs can be seen as a signature of the degree of coherence in the system.

Figure 4.13: The LG parameter K_+ for different values of the squeezing parameter s. Here, $\beta = 100$. $\omega_0 = 0.5$, $R = 0.05$. Further, $s = 0, 1$ and 3.5 correspond to $\mu_s = 1, 0.9$ (underdamped) and $6.7i$ (overdamped), respectively.

In the strong driving limit, i.e., $\Omega \gg \gamma_s$, the LG parameters are given by Eq. (4.52) and are plotted in Fig. 4.11. The parameters K_+ and K_- show complementary behavior in the sense that when one of these parameters does not show a violation, the other does, together covering the entire parameter range. The interaction with the squeezed thermal reservoir leads to enhancement in the transition rate which is given by $\gamma = \gamma_0(2n+1)$, where γ_0 is the spontaneous emission rate and $\gamma_0 n$ is the squeezed thermal induced emission and absorption rate. The decoherence effects arising due to interaction with the environment are expected to decrease the quantumness in the system. This feature is depicted in Fig. 4.12, where K_+ shows enhanced violations for larger values of the parameter β i.e, for smaller temperature, where decoherence is expected to be lesser. The squeezing parameter as defined in Eq. (4.33), controls the degree of violation of LGtIs, since it affects the total photon distribution. Figure 4.13 exhibits the variation of the LG parameter K_+ for different values of squeezing parameter s. The increase in s is found to decrease the extent of violation of LGtI. The effect of weak measurement on the LG parameters is depicted in Fig. 4.14. The ideal projective measurements are characterized by $\xi = 1$, while $\xi = 0$ corresponds to no measurement. It is clear from the figure that the maximum violation occurs for ideal projective measurements.

In [277], general evolution of an atom in squeezed vacuum was analyzed and the experimental studies of two level systems in vacuum were reported in [278, 279]. Here, consideration of the effect of various parameters such as temperature and external driving on the LGtI violation helps in developing a better understanding of the quantumness of the system under consideration, under ambient conditions.
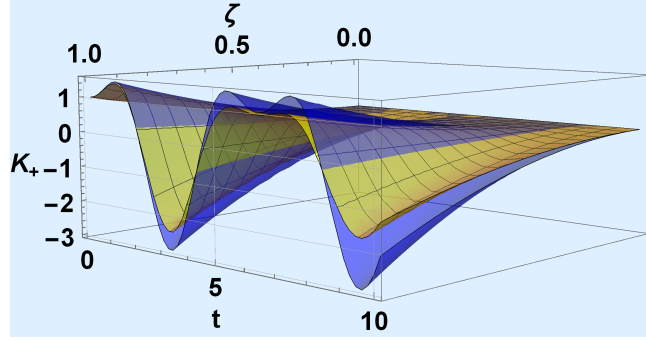
Figure 4.14: Variation of LG parameter K_+ with respect to t and ξ. With $\beta = 5$, $\omega_0 = 0.5$ and $s = 0$, we have $R = 0$ ($\mu_s \approx 1$) depicted by blue plane-surface, $R = 0.05$ ($\mu_s \approx 0.9$) represented by yellow lined-surface. Both these correspond to underdamped case. The maximum violation corresponds to $\xi = 1$, the ideal projective measurement.

4.4 Study of coherence based measure in (non) Markovian channels

This section makes a detailed analysis of quantumness for various quantum noise channels, both Markovian and non-Markovian, and follows [107]. The noise channels considered include dephasing channels like random telegraph noise, non-Markovian dephasing and phase damping, as well as the non-dephasing channels such as generalized amplitude damping and Unruh channels. We study a recently introduced witness for quantumness based on the square l_1 norm of coherence. It is found that the increase in the degree of non-Markovianity increases the quantumness of the channel. This may be attributed to the fact that the non-Markovian dynamics involves the generation of entanglement between the system and environment degrees of freedom.

Quantum coherence [84, 280] is central to quantum mechanics, playing a fundamental role for the manifestations of quantum properties of a system. It is at the heart of the phenomena such as multi-particle interference and entanglement which are pivotal for carrying out various quantum information and communication tasks, viz., quantum key distribution [281, 282] and teleportation [141]. An operational formulation of coherence as a resource theory was recently developed [283]. The notion of coherence [284] has its roots in quantum optics [2, 285]. Recent developments have made use of coherence in superconducting systems [286], biological systems [287], non-Markovian phenomena [288], foundational issues [88, 289] and subatomic physics [8, 290].

Quantum channels are completely positive (CP) and trace preserving (TP) maps between the spaces of operators and describe processes like transmission of classical as well as quantum information. Quantum information protocols are based on the fact that information is transmitted in the form of quantum states. This is achieved either by directly sending non-orthogonal states or by using pre-shared entanglement. The channels can reduce the degree of coherence and entanglement as the information flows from sender to receiver. Interestingly, it was shown in [291] that quantum channels can have cohering power and that a qubit unitary map has equal cohering and decohering power in any basis. In general, the extent to which the quantum features are affected depends on the underlying dynamics and the type of noise. Therefore it is natural to ask to what extent is coherence preserved by a channel used to transmit quantum information.

The physical foundation of a large number of quantum channels relies on the Born-Markov approximations [110]. However, in a number of quantum communication tasks, the characteristic time scales of the system of interest become comparable with the reservoir correlation time. Therefore, a non-Markovian description for such scenarios becomes indispensable [58]. The re-

liability of a quantum channel is tested by the probability that the output and input states are the same. A well known measure to quantify the performance of a channel is the *average fidelity* [292–295]. The notion of *fidelity* of two quantum states provides a qualitative measure of their distinguishability [296]. Recently, a measure based on Fisher information was introduced to quantify the invasiveness of quantum channels [297]. In [298], a witness of nonclassicality of a channel was introduced. This is based on average quantum coherence of the state space, using the square l_1 norm of coherence of qubit channels. It was shown that the extent to which quantum correlation is preserved under local action of the channel cannot exceed the quantumness of the underlying channel.

We use the definition of quantumness based on the average coherence and apply it to different channels, both Markovian and non-Markovian. Being a quantitative measure of the "closeness" of the output and input states, average channel fidelity is a useful figure of merit when considering channel transmission [299], particularly in the presence of noise. Accordingly, a corresponding study is made on these channels. We proceed as follows. In subsection 4.4.1, we briefly review the definition of nonclasscality of quantum channels. Subsection 4.4.2 is devoted to analyzing the interplay of quantumness and average fidelity in various noise models. Results and their discussion is made in Sec. 4.4.3.

4.4.1 A coherence based measure of quantumness of channels

Here, we study a coherence based measure introduced in [298], and given by

$$Q_C(\Phi) = N_C \min_{|i\rangle} \int C(\Phi(\rho)) d\mu(\rho). \tag{4.57}$$

Here, Φ is the channel under consideration, C denotes the chosen measure of coherence, N_C is a normalization constant and $\mu(\rho)$ is the Haar measure. The minimization is performed over all orthonormal states $\{|i\rangle\}$ to ensure the defined measure is a basis independent quantity. To proceed, we analyze the effect of a qubit channel on a state $\boldsymbol{\rho} = \frac{1}{2}(\boldsymbol{I} + \boldsymbol{\xi}\boldsymbol{\sigma})$. The Bloch vector ξ transforms as

$$\Phi(\boldsymbol{\rho}) = \boldsymbol{\rho}' = \frac{1}{2}(\boldsymbol{I} + \boldsymbol{\xi}'\boldsymbol{\sigma}). \tag{4.58}$$

Here, $\boldsymbol{\xi}' = \boldsymbol{A}\boldsymbol{\xi} + \boldsymbol{B}$, such that the matrices $\mathbf{A}_{3\times3}$ and $\mathbf{B}_{3\times1}$ depend on the channel parameters. By choosing the square l_1-norm as the measure of coherence, we compute the coherence with respect to an arbitrary orthonormal basis. The l_1-norm of coherence C_{l_1} is often used as a coherence measure, since it is easy to compute and algebraically easy to manipulate [300]. Further, C_{l_1} links different coherence and entanglement measures. For example, C_{l_1} is the upper bound for another important coherence measure called *robustness of coherence* for all qubit states [301]. It is also useful in studying Deutsch-Jozsa algorithm [302, 303] and Grover algorithm [304, 305]. It plays an important role in quantifying the cohering and decohering powers of quantum operations [306], and also corresponds to the maximum entanglement generated by incoherent operations acting on the system and an incoherent ancilla [307].

To make the quantumness witness a basis independent quantity, one performs optimization over all orthonormal basis, leading to a closed expression for the quantumness witness

$$Q_{C_{l_1}^2}(\Phi) = \lambda_2 + \lambda_3. \tag{4.59}$$

Here, $\lambda_1 \geq \lambda_2 \geq \lambda_3$ are eigenvalues of matrix $\boldsymbol{\mathcal{L}} = \frac{1}{2}(\boldsymbol{A}\boldsymbol{A}^T + 5\boldsymbol{B}\boldsymbol{B}^T)$, with T denoting the transpose operation. Thus, Eq. (4.59) gives an operational definition of the quantumness of a channel. In what follows, we will drop the subscript $C_{l_1}^2$ and call the quantumness of a map Φ just as $Q(\Phi)$. It is worth mentioning here, that for the unital channels, which map identity to identity, i.e., $\Phi(\boldsymbol{I}) = \boldsymbol{I}$, the above definition of quantumness coincides with the geometric discord [298].

4.4.2 Specific channels

A brief account of various quantum channels [299, 308] used in this work is presented here. The dephasing channels include random telegraph noise (RTN) [95, 309], non-Markovian dephasing (NMD) [97] and phase damping (PD) [87] channels while in the non-dephasing class, we consider generalized amplitude damping (GAD) [80, 92] and Unruh channels [310].

Random Telegraph Noise: This channel characterizes the dynamics when the system is subjected to a bi-fluctuating classical noise, generating RTN with pure dephasing. The dynamical map acts as follows

$$\Phi^{RTN}(\boldsymbol{\rho}) = \boldsymbol{\mathcal{R}}_0 \boldsymbol{\rho} \boldsymbol{\mathcal{R}}_0^\dagger + \boldsymbol{\mathcal{R}}_1 \boldsymbol{\rho} \boldsymbol{\mathcal{R}}_1^\dagger, \qquad (4.60)$$

where the two Kraus operators are given by

$$\boldsymbol{\mathcal{R}}_0 = \sqrt{\frac{1 + \Lambda(t)}{2}} \boldsymbol{I}, \qquad \boldsymbol{\mathcal{R}}_1 = \sqrt{\frac{1 - \Lambda(t)}{2}} \boldsymbol{\sigma}_z. \qquad (4.61)$$

Here, $\Lambda(t)$ is the *memory kernel*

$$\Lambda(t) = e^{-\gamma t} \left[\cos \left[\sqrt{\left(\frac{2b}{\gamma}\right)^2 - 1} \, \gamma t \right] + \frac{\sin \left[\sqrt{\left(\frac{2b}{\gamma}\right)^2 - 1} \, \gamma t \right]}{\sqrt{\left(\frac{2b}{\gamma}\right)^2 - 1}} \right], \qquad (4.62)$$

where b quantifies the system-environment coupling strength and γ is proportional to the fluctuation rate of the RTN. Also, $\boldsymbol{I}$ and $\boldsymbol{\sigma}_z$ are the identity and Pauli spin matrices, respectively. The completeness condition reads $\boldsymbol{\mathcal{R}}_0 \boldsymbol{\mathcal{R}}_0^\dagger + \boldsymbol{\mathcal{R}}_1 \boldsymbol{\mathcal{R}}_1^\dagger = \boldsymbol{I}$. The dynamics is Markovian [non-Markovian] if $(4b\tau)^2 > 1$ [$(4b\tau)^2 < 1$], where $\tau = 1/(2\gamma)$. Starting with the state $\boldsymbol{\rho} = \frac{1}{2}(\boldsymbol{I} + \boldsymbol{\xi}\boldsymbol{\sigma})$, the new Bloch vector is given by $\boldsymbol{\xi}' = [\boldsymbol{\xi}_x \Lambda(t), \boldsymbol{\xi}_y \Lambda(t), \boldsymbol{\xi}_z]^T$. This implies $\boldsymbol{A} = \text{diag.}[\Lambda(t), \Lambda(t), 1]$ and $\boldsymbol{B} = 0$, and consequently, $\boldsymbol{\mathcal{L}} = \text{diag.}[\frac{1}{2}[\Lambda(t)]^2, \frac{1}{2}[\Lambda(t)]^2, \frac{1}{2}]$. Since, $-1 \leq \Lambda(t) \leq 1$, we identify both the small eigenvalues as $\frac{1}{2}[\Lambda(t)]^2$, leading to

$$Q(\Phi^{RTN}) = [\Lambda(t)]^2. \qquad (4.63)$$

We, next compute the fidelity for the states $\boldsymbol{\rho}$ and $\boldsymbol{\rho}'$, the initial and final states, respectively. This will be followed by a study of its interplay with quantumness. The fidelity between qubit states $\boldsymbol{\rho}$ and $\boldsymbol{\rho}'$ is [296]

$$F(\boldsymbol{\rho}, \boldsymbol{\rho}') = Tr[\boldsymbol{\rho}\boldsymbol{\rho}'] + 2\sqrt{Det[\boldsymbol{\rho}]Det[\boldsymbol{\rho}']}. \qquad (4.64)$$

Using a general qubit parametrization

$$\boldsymbol{\rho} = \begin{bmatrix} \cos^2(\theta/2) & \frac{1}{2}e^{-i\phi}\sin(\theta) \\ \frac{1}{2}e^{i\phi}\sin(\theta) & \sin^2(\theta/2) \end{bmatrix}, \qquad (4.65)$$

the fidelity for RTN model turns out to be

$$F_{RTN} = \frac{1}{4}\left[3 + \cos(2\theta) + 2\sin^2(\theta)\Lambda(t)\right]. \qquad (4.66)$$

In order to make this quantity state independent, we calculate the *average* fidelity $\mathcal{F} = \frac{1}{4\pi}\int_0^{2\pi}\int_0^{\pi} F \sin(\theta)d\theta d\phi$. We have

$$\mathcal{F}_{RTN} = \frac{1}{3}[2 + \Lambda(t)]. \qquad (4.67)$$

Since $-1 \leq \Lambda(t) \leq 1$, the average fidelity is symmetric about its classical value $2/3$.

Non-Markovian dephasing: This channel is an extension of the dephasing channel to non-Markovian class. The non-Markovianity is identified with the appearance of a not completely positive (NCP) intermediate map [97]. The Kraus operators are given by

$$\boldsymbol{\mathcal{N}}_0 = \sqrt{(1 - \alpha p)(1 - p)} \, \boldsymbol{I},$$
$$\boldsymbol{\mathcal{N}}_1 = \sqrt{p + \alpha p(1 - p)} \, \boldsymbol{\sigma}_z. \qquad (4.68)$$
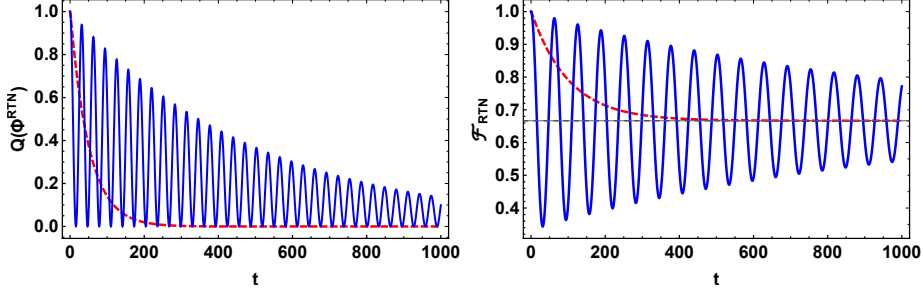
Figure 4.15: RTN channel: The quantumness $Q(\Phi^{RTN})$ Eq. (4.63) and *average* fidelity $\mathcal{F}_{RTN}$ Eq. (4.67), plotted with respect to time t (sec.), for a qubit subjected to RTN. The solid (blue) and dashed (red) curves correspond to non-Markovian ($b = 0.05$, $\gamma = 0.001$) and Markovian ($b = 0.07$, $\gamma = 1$) cases, respectively. The fidelity oscillates symmetrically about $2/3$ in non-Markovian case, while in Markovian case, it decreases monotonically and saturates to this value.
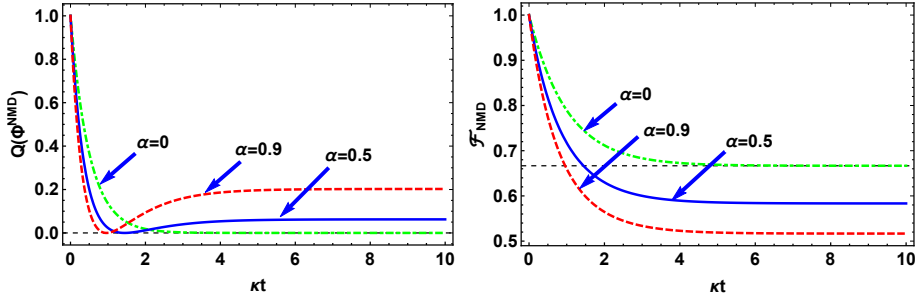

Figure 4.16: NMD channel: The quantumness $Q(\Phi^{NMD})$ Eq. (4.69) and *average* fidelity $\mathcal{F}_{NMD}$ Eq. (4.70), plotted with respect to the dimensionless parameter κt, for a qubit subjected to NMD, for different values of parameter α.

Here, the parameter α quantifies the degree of non-Markovianity of the channel, such that $\alpha = 0$ corresponds to conventional dephasing, while as α increases, the non-Markovian behavior correspondingly increases. Further, p is a time-like parameter such that $0 \leq p \leq 1/2$. In this case, the quantumness parameter turns out to be

$$Q(\Phi^{NMD}) = \Omega^2(p), \tag{4.69}$$

where $\Omega = 1 - 2p - 2\alpha p(1 - p)$. The average fidelity, in this case, is given by

$$\mathcal{F}_{NMD} = \frac{1}{3}[2 + \Omega(p)]. \tag{4.70}$$

We use the parametrization $p = \frac{1}{2}(1 - e^{-\kappa t})$, such that as $t : 0 \to \infty$, $p : 0 \to 1/2$.

Phase damping (PD) channel: PD channel models the phenomena where decoherence occurs without dissipation (loss of energy). The dynamical map, in this case has the Kraus representation

$$\mathcal{P}_0 = \begin{bmatrix} 1 & 0 \\ 0 & \sqrt{1-S} \end{bmatrix}, \qquad \mathcal{P}_1 = \begin{bmatrix} 0 & 0 \\ 0 & \sqrt{S} \end{bmatrix}. \tag{4.71}$$

The parameter S can be modeled by the following time dependence $S = 1 - \cos^2(\chi t)$, for $0 \leq \chi t \leq \pi/2$. The quantumness parameter, in this case, is given by
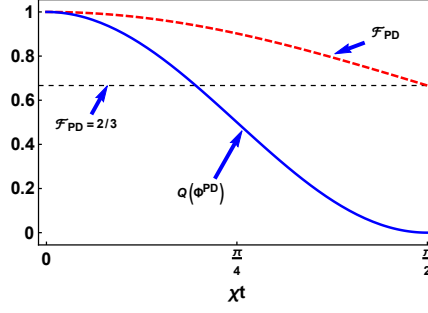
$$Q(\Phi^{PD}) = 1 - S = \cos^2(\chi t). \tag{4.72}$$

Figure 4.17: PD channel: The quantumness $Q(\Phi^{PD})$ Eq. (4.72) and *average* fidelity $\mathcal{F}_{PD}$ Eq. (4.73), plotted with respect to the dimensionless quantity χt, for a qubit subjected to PD noise.
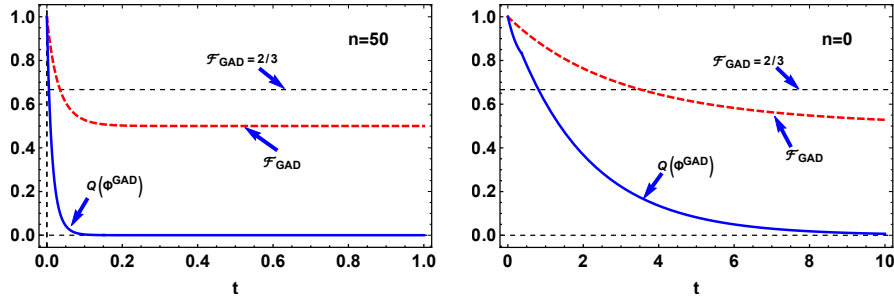

Figure 4.18: GAD channel: The quantumness $Q(\Phi^{GAD})$ Eq. (4.75) and fidelity $\mathcal{F}_{GAD}$ Eq. (4.76), plotted with respect to time t (sec.), for a qubit subjected to GAD noise. With $\gamma = 1$, the left and right panels correspond to the cases when $n = 50$ and 0, respectively. Here, $\tau \approx 0.1246$ and 0.3646 in the former and later case, respectively. The $n = 0$ case corresponds to the zero temperature limit, such that GAD reduces to AD noise.

The average fidelity turns out to be

$$\mathcal{F}_{PD} = \frac{1}{3}[2 + \cos(\chi t)]. \tag{4.73}$$

Generalized Amplitude Damping (GAD) channel: GAD is a generalization of the AD channel to finite temperatures [58]. The later models processes like spontaneous emission from an atom and is pertinent to the problem of quantum erasure [168]. The dynamics, in this case, is governed by the following Kraus operators

$$\mathcal{A}_0 = \begin{bmatrix} \sqrt{\Theta} & 0 \\ 0 & \sqrt{s\Theta} \end{bmatrix}, \quad \mathcal{A}_1 = \begin{bmatrix} 0 & \sqrt{p\Theta} \\ 0 & 0 \end{bmatrix},$$

$$\mathcal{A}_2 = \begin{bmatrix} \sqrt{s(1-\Theta)} & 0 \\ 0 & \sqrt{(1-\Theta)} \end{bmatrix}, \quad \mathcal{A}_3 = \begin{bmatrix} 0 & 0 \\ \sqrt{p(1-\Theta)} & 0 \end{bmatrix}. \tag{4.74}$$

Here, $\Theta = \frac{n+1}{2n+1}$, and $s = \exp[-\frac{\gamma t}{2}(2n+1)]$. Also, n is the mean number of excitations in the bath and γ represents the spontaneous emission rate. In the zero temperature limit, $n = 0$, implying $\Theta = 1$, thereby recovering the AD channel. The quantumness parameter for GAD channel comes out to be

$$Q(\Phi^{GAD}) = \begin{cases} \frac{1}{2}s + \tilde{s} & \text{for } t \le \tau, \\[2mm] s & \text{for } t > \tau. \end{cases} \tag{4.75}$$
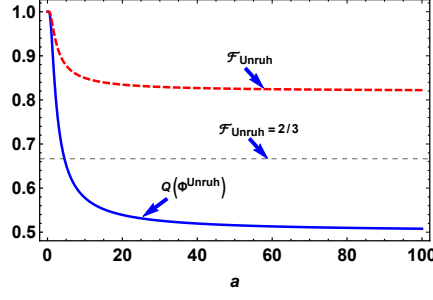
61

Figure 4.19: Unruh channel: The behavior of quantumness and average fidelity depicted with respect to the acceleration a (in units $\hbar = c = 1$).

with,

$$\tilde{s} = \frac{5}{2}(2\Theta - 1)^2(1 - s)^2,$$

$$\tau = -\frac{2}{\gamma(2n + 1)} \ln\left[\frac{5}{6 + 4n + n^2}\right].$$

The average fidelity in this case is given by

$$\mathcal{F}_{GAD} = \frac{1}{6}[3 + 2\sqrt{s} + s]. \tag{4.76}$$

Here $s = \exp[-\frac{\gamma t}{2}(2n + 1)]$.

Unruh channel: To an observer undergoing acceleration a, the Minkowski vacuum appears as a warm gas emitting black-body radiation at temperature given by $T = \frac{\hbar a}{2\pi c K_B}$, called the *Unruh temperature* and the effect is known as the *Unruh effect*. The Unruh effect has been described as a noisy quantum channel with the following Kraus operators

$$\mathbf{U}_0 = \begin{bmatrix} \cos(r) & 0 \\ 0 & 1 \end{bmatrix} \quad \text{and} \quad \mathbf{U}_1 = \begin{bmatrix} 0 & 0 \\ \sin(r) & 0 \end{bmatrix}. \tag{4.77}$$

Here, $\cos(r) = [1 + \exp(-2\pi c\omega/a)]^{-1/2}$. The quantumness parameter for the Unruh channel turns out to be

$$Q(\Phi^{\text{Unruh}}) = \cos^2(r). \tag{4.78}$$

The average fidelity here is

$$\mathcal{F}_{\text{Unruh}} = \frac{1}{12}(4\cos(r) + \cos(2r) + 7). \tag{4.79}$$

4.4.3 Results and discussion

The quantumness of noisy channels is quantified by the coherence measure given by Eq. (4.57). For specific case of a two level system (qubit), using square l_1 norm as a measure of coherence, one obtains a simple working rule for computing the quantumness of a channel, given in Eq. (4.59).

For RTN channel, the quantumness measure turns out to be the square of the memory kernel $\Lambda(t)$, defined in Eq. (4.62). In the non-Markovian regime, both the quantumness as well as

fidelity are seen to sustain much longer in time as compared with the Markovian case, Fig. 4.15. In the limit $t \to \infty$, $\Lambda(t) \to 0$, consequently, we have

$$Q(\Phi^{RTN}) = \Lambda^2(t) \to 0, \text{ and } \mathcal{F}_{RTN} = \frac{1}{3}(2 + \Lambda(t)) \to \frac{2}{3}. \tag{4.80}$$

This is consistent with our notion of fidelity less than or equal to $2/3$ for a processes that can be simulated by a classical theory. The NMD channel shows non-zero quantumness within the allowed range, i.e., $[0, 1/2]$, of time like parameter p, for $0 < \alpha \le 1$. In this case, the parameter α quantifies the degree of non-Markovianity, which increases as α goes from 0 to 1. At $p = 1/2$, i.e., for $t \to \infty$, $\Omega(p) = -\alpha/2$, we have

$$Q(\Phi^{NMD}) = \alpha^2/4 \quad \text{and} \quad \mathcal{F}_{NMD} = \frac{2}{3}(1 - \alpha/2) \tag{4.81}$$

That is, the quantumness parameter is always positive but the average fidelity goes below its classical limit. This is consistent with [298] that a nonzero value of the coherence based measure of quantumness is a necessary but not sufficient criterion for quantum advantage in teleportation fidelity. This is also consonant with the use of fidelity as a tool to assess quantumness [311]. However, in the Markovian limit, i.e., $\alpha \to 0$, $\Omega \to 1 - 2p$. Since $p \in [0, 1/2]$, implies $\Omega \in [0, 1]$. Therefore, $Q(\Phi^{NMD}) = (1 - 2p)^2$ and $\mathcal{F}_{NMD} = \frac{1}{3}[2 + (1 - 2p)]$, both the quantities lead to similar predictions in this limit. These features are depicted in Fig. 4.16.

One of the purely quantum noise channels is the PD channel which characterizes the processes accompanied with the loss of coherence without loss of energy. The behavior of quantumness and average fidelity, in this case, is depicted in Fig 4.17. The parameter $Q(\Phi^{PD})$ becomes zero as $\mathcal{F}_{PD}$ reaches $2/3$.

Next we analyzed non-dephasing models such as GAD and Unruh channels. From the GAD channel, one can recover the AD channel in the zero temperature limit, i.e., when $n = 0$, see Eq. (4.74). In this case $\Theta = 1$ and the quantumness parameter, with $\xi = 1 - s$, becomes

$$Q(\Phi^{AD}) = \begin{cases} \frac{1}{2}[6\xi^2 - 3\xi + 2] & \text{for } \xi \le 1/6, \\[2ex] 1 - \xi & \text{for } \xi > 1/6. \end{cases} \tag{4.82}$$

This is consistent with the results given in [298]. In the case of GAD channel, the quantumness parameter is nonzero even though the average fidelity goes below its classical limit $2/3$. This reiterates the statement made earlier regarding quantumness and average teleportation fidelity, Fig. 4.18. In the high temperature regime, both the measures, i.e., quantumness as well as average fidelity seem to lead to similar predictions at the same time. For Unruh channel, the quantumness and average fidelity are studied with respect to the acceleration a. Both the measures show a saturation at values which are well above their classical limits, Fig 4.19. This is in consonance with [310], where it was shown that the Unruh channel, though structurally similar to the AD channel, is different from it.

4.5 A proposed measure of quantumness of channels

In this section, we discuss a measure of quantumness of channels based on an intuitive approach, proposed in [108]. It is easy to compute and amenable to experimental verification.

Quantifying the degree of quantumness of a channel has both theoretical and practical significance in quantum information science [4]. The quantum channels are completely positive

and trace preserving maps which describe processes like information transfer in a given environment [109]. Since quantum information is transmitted in the form of quantum states, it is important to quantify the degree to which a quantum state gets affected while subjected to a quantum channel [110]. The classical states are usually identified as those whose correlations can be described in terms of classical probabilities. This approach has lead to the quantification of some well known nonclassical correlations such as entanglement, discord and related quantities [111]. Alternatively, a different way of quantifying the quantumness of a single system is by exploiting the non-commutative algebra of observables, such that the mutual commutation of all the accessible states of the system identify with a classical system. This approach has advantages in that it make no reference to the correlations and no complicated optimization procedures are needed [112].

Noise is usually known for its negative role in reducing the degree of coherence in a system. However, they can show enhancement in nonclassical correlations for some states [92, 113, 114]. In [115–117], it was shown that local environments can enhance the average fidelity of quantum teleportation for certain entangled states. Enhancement in quantum discord by local Markovian (i.e., memoryless) noise channels was reported in [118, 119]. Quantum channels provide a platform for studying the interplay between quantumness of states and the underlying dynamics in presence of an ambient environment [58]. This has lead to several interesting observations. For example, in [120] it was shown that the quantum channels need not be decohering, but could have cohering power as well. The cohering power, that is, the ability of quantum operations to produce coherence, was given an operational interpretation in [121]. It was further shown that the cohering power of any quantum operation is upper bounded by the corresponding unitary operation. The entangling capabilities of unitary operations acting on bipartite systems was reported in [122], with the maximum entanglement being created with product input states [123]. The deteriorating effect of the environment on a quantum state has been studied in the context of coherence-breaking channels and coherence sudden death [124]. An interesting class of channels known as semi-classical channels Λ_{SC} map all the input states ρ to $\Lambda_{SC}(\rho)$, such that the later are diagonal in the same basis. Such channels are realized by complete decoherence after which only diagonal elements of the density matrix are non-zero [125]. Another well studied class of quantum channels are those based on Lindbladian evolution which focus on the dynamics at time scales well separated from that of the reservoir correlations. However, in a number of practical applications, this assumption is not true and one has to take into account the non-Markovian aspects of the underlying dynamics [95, 97]. In [126–128], coherence of quantum channels was analyzed using Choi-Jamiolwski isomorphism.

Recently, a coherence based measure of quantumness of channel was proposed in [298], by defining the measure as the average quantum coherence of the state after the quantum channel acts on it, and minimized over all orthonormal basis sets of the state space. This measure was studied in the context of various (non) Markovian channels [107]. Further, this measure connects different coherence and entanglement measures, and is also the upper bound for another important coherence measure called *robustness of coherence* for all qubit states [301].

Here, we discuss a simple measure for quantumness of channels, based on commutation properties of the states evolving under the relevant channels proposed in [108]. A necessary and sufficient condition for the creation of quantum correlations via local channels in finite dimensions is that they should not be *commutativity preserving* [312]. Commutative quantum channels preserve the commutation relation of any two compatible states, i.e., if $[\rho, \sigma] = 0$, then $[\mathcal{E}(\rho), \mathcal{E}(\sigma)] = 0$. It is clear that the semiclassical channels, defined above, are commutativity preserving, implying that a departure from semiclassicality is necessary to create quantum correlations.

This section is organized as follows: In subsection 4.5.1 we introduce a measure of quantumness of channels. Subsection 4.6 is devoted to applying this measure to various well known quantum channels. The experimental relevance of this measure is discussed in subsection 4.7. Results and their discussion are presented in Sec. 4.8.

4.5.1 Measure of quantumness of channels

Given two *arbitrary* states ρ and σ, one can quantify their mutual incompatibility by the Hilbert-Schmidt (HS) norm of their commutator $\mathcal{M}(\rho, \sigma) = 2\|\,C\,\|_{HS} = 2\,\mathrm{Tr}[C^\dagger\,C]$. The measure is defined in terms of the HS norm of their commutator $C = \rho\sigma - \sigma\rho$. The HS norm for an operator O is defined as $\|\,O\,\|_{HS}^2 = \mathrm{Tr}[O^\dagger\,O]$. This measure was motivated in [112] with the aim of identifying nonclassicality with the incompatibility of states. Consider two qubit states $\rho_a = \frac{1}{2}(1 + \vec{a} \cdot \vec{\sigma})$ and $\rho_b = \frac{1}{2}(1 + \vec{b} \cdot \vec{\sigma})$, with $\vec{a}, \vec{b} \in \mathbb{R}^3$ and $\vec{\sigma} = (\sigma_x, \sigma_y, \sigma_z)$ represents the three Pauli spin matrices. We have $\rho_a\rho_b - \rho_b\rho_a = i\frac{1}{2}(\vec{a} \times \vec{b}) \cdot \vec{\sigma}$, and

$$\mathcal{M}(\rho_a, \rho_b) = 2\,\mathrm{Tr}\{(\rho_a\rho_b - \rho_b\rho_a)^\dagger(\rho_a\rho_b - \rho_b\rho_a)\} = |\vec{a} \times \vec{b}|^2. \tag{4.83}$$

This quantify vanishes for orthogonal $\vec{a}$ and $\vec{b}$ and attains its maximum value of one when $\vec{a}$ and $\vec{b}$ are parallel, $0 \le \mathcal{M}(\rho, \sigma) \le 1$.

Here we try to exploit this approach to probe the quantumness of a channel. Consider a channel described by a linear, completely positive and trace preserving map $\Phi : L(\mathcal{H}_A) \to L(\mathcal{H}_B)$ [280, 308]. The action of this map on an input state ρ leads to an output state ρ' and can be summarized as

$$\rho' = \Phi[\rho]. \tag{4.84}$$

In the context of quantum channels, we start with two states ρ_a and ρ_b which are maximally noncommuting in the sense that $\mathcal{M}(\rho_a, \rho_b) = 1$. By subjecting these states to a quantum channel, the quantumness of the channel can be attributed to the extent to which ρ'_a and ρ'_b (the outputs) are incompatible

$$\mathcal{M}(\rho'_a, \rho'_b) = 2\|\,C\,\|_{HS}^2 = 2\,\mathrm{Tr}[C^\dagger\,C], \tag{4.85}$$

with $C = \rho'_a\rho'_b - \rho'_b\rho'_a$. This quantity when maximized over all input states serves as a measure for the quantumness of the channel

$$\mu = \max_{\rho_a, \rho_b} \mathcal{M}(\rho'_a = \Phi[\rho_a], \rho'_b = \Phi[\rho_b]). \tag{4.86}$$

As an example, consider the states $|a\rangle = \cos(x/2)\,|0\rangle + e^{-i\phi}\sin(x/2)\,|1\rangle$ and $|b\rangle = \cos(y/2)\,|0\rangle + e^{-i\xi}\sin(y/2)\,|1\rangle$, with the respective density matrix representations

$$\rho_a = \frac{1}{2}(1 + \vec{a} \cdot \vec{\sigma}) = \begin{pmatrix} \cos^2(x/2) & e^{i\phi}\frac{\sin(x)}{2} \\ e^{-i\phi}\frac{\sin(x)}{2} & \sin^2(x/2) \end{pmatrix},$$

$$\rho_b = \frac{1}{2}(1 + \vec{b} \cdot \vec{\sigma}) = \begin{pmatrix} \cos^2(y/2) & e^{i\phi}\frac{\sin(y)}{2} \\ e^{-i\xi}\frac{\sin(y)}{2} & \sin^2(y/2) \end{pmatrix}. \tag{4.87}$$

Here, $\vec{a}, \vec{b} \in \mathbb{R}^3$ are the Bloch vectors and $\vec{\sigma} = (\sigma_x, \sigma_y, \sigma_z)$ represents the Pauli matrix triplet. The states ρ_a and ρ_b are maximally non-commuting for $y = x + \pi/2$ and $\xi = \phi$, as can be seen by calculating the commutator

$$C = \rho_a\rho_b - \rho_b\rho_a = \begin{pmatrix} 0 & \frac{e^{i\phi}}{2} \\ -\frac{e^{-i\phi}}{2} & 0 \end{pmatrix}. \tag{4.88}$$

Therefore $\mathcal{M}(\rho_a, \rho_b) = 2\,\mathrm{Tr}[C^\dagger\,C] = 1$. Thus the states are maximally noncommuting and in this sense share maximum nonclassicality. In this example, no optimization is required since the quantity $\mathcal{M}(\rho_a, \rho_b)$ is independent of input state parameters. However, as discussed ahead, subjecting these states to quantum channels can make $\mathcal{M}(\rho_a, \rho_b)$ dependent on input state parameters. In such cases, we need to maximize over all such parameters to compute the degree of incompatibility of the output states.

4.6 Application to quantum channels

We will now apply the above definition to some well known quantum channels. We consider the dephasing channels like random telegraph noise (RTN) [309], non-Markovian dephasing (NMD) [313], phase damping (PD) [87] and generalized depolarizing channel (GDC) [314]. The generalized amplitude damping channel (GAD) [80, 92], which represents a dissipative channel is also studied. The Kraus operators for these channels are given in Table (4.2).

Example 1. Random Telegraph Noise (RTN): The dynamical map is represented by the Kraus operators $K_0(t) = k_+\,\mathbf{I}$ and $K_1(t) = k_-\,\sigma_z$, where $k_\pm = \sqrt{\frac{1\pm\Lambda(t)}{2}}$, such that the action on a general qubit state

$$\rho = \begin{pmatrix} 1-p & x \\ x^* & p \end{pmatrix}, \qquad (4.89)$$

is given by

$$\rho' = \Phi^{RTN}\begin{pmatrix} 1-p & x \\ x^* & p \end{pmatrix} = \begin{pmatrix} 1-p & x\Lambda(t) \\ x^*\Lambda(t) & p \end{pmatrix}. \qquad (4.90)$$

Let us use the maximally nonclassical pair of states given in Eq. (4.87). The states ρ_a and ρ_b, defined in Eq. (4.87) are subjected to RTN evolution

$$
\begin{aligned}
\rho_a' &= \begin{pmatrix} \cos^2\left(\frac{x}{2}\right) & \frac{1}{2}e^{i\phi}\sin(x)\Lambda(t) \\ \frac{1}{2}e^{-i\phi}\sin(x)\Lambda(t) & \sin^2\left(\frac{x}{2}\right) \end{pmatrix}, \\
\rho_b' &= \begin{pmatrix} \cos^2\left(\frac{1}{4}(2x+\pi)\right) & \frac{1}{2}e^{i\phi}\cos(x)\Lambda(t) \\ \frac{1}{2}e^{-i\phi}\cos(x)\Lambda(t) & \sin^2\left(\frac{1}{4}(2x+\pi)\right) \end{pmatrix}.
\end{aligned}
\qquad (4.91)
$$

The pertinent commutator in this case becomes

$$C = \begin{pmatrix} 0 & \frac{1}{2}e^{i\phi}\Lambda(t) \\ -\frac{1}{2}e^{-i\phi}\Lambda(t) & 0 \end{pmatrix}. \qquad (4.92)$$

Therefore, the quantumness measure for the RTN channel turns out to be $\mu = \max_{\rho_1,\rho_2}\mathcal{M}(\rho_a', \rho_b') = 2\,\mathrm{Tr}[C^\dagger\,C] = [\Lambda(t)]^2$.

Example 2. Generalized depolarizing channel (GDC): The generalized depolarizing channel is represented by the following Kraus operators $M_i = \sqrt{p_i}\sigma_i$ with $i = 0, 1, 2, 3$, where σ_i are the Pauli matrices. The states ρ_a and ρ_b given by Eq. (4.87) evolve under the action of this channel such that the new Bloch vectors are given by

$$
\begin{aligned}
\vec{a} &= \begin{pmatrix} (p_0 + p_1 - p_2 - p_3)\sin x\cos\phi \\ (-p_0 + p_1 - p_2 + p_3)\sin x\sin\phi \\ (p_0 - p_1 - p_2 + p_3)\cos x \end{pmatrix} \\
\vec{b} &= \begin{pmatrix} (p_0 + p_1 - p_2 - p_3)\cos x\cos\phi \\ (-p_0 + p_1 - p_2 + p_3)\cos x\sin\phi \\ (-p_0 + p_1 + p_2 - p_3)\sin x \end{pmatrix}
\end{aligned}
\qquad (4.93)
$$

Therefore,

$$
\begin{aligned}
\mathcal{M}(\rho'_a, \rho'_b) &= |\vec{a} \times \vec{b}|, \\
&= (p_0 - p_1 - p_2 + p_3)^2 [2(p_0 - p_3)(p_1 - p_2)\cos(2\phi) + (p_0 - p_3)^2 + (p_1 - p_2)^2].
\end{aligned}
\tag{4.94}
$$

This is maximum for $\phi = 0$, i.e., $\mu = \mathcal{M}(\rho'_a, \rho'_b)|_{\phi=0} = (p_0 + p_1 - p_2 - p_3)^2 (p_0 - p_1 - p_2 + p_3)^2$.

4.7 Experimental relevance of the measure

It is important to note that the quantity $\mathcal{M}(\rho'_a, \rho'_b)$ can be given an experimental interpretation using an interferometric setup [315]. This useful technique can be easily incorporated to our purpose of quantifying quantumness of channels. One can write

$$
\mu = \max_{\rho_a, \rho_b} \mathcal{M}(\rho'_a, \rho'_b) = 4 \max_{\rho_a, \rho_b} \mathrm{Tr}[(\rho'_a)^2 (\rho'_b)^2 - (\rho'_a \rho'_b)^2].
\tag{4.95}
$$

The two quantities $\mathrm{Tr}[(\rho'_a)^2 (\rho'_b)^2]$ and $\mathrm{Tr}[(\rho'_a \rho'_b)^2]$ can be obtained from two separate measurements. The input state $\rho = |0\rangle\langle 0| \otimes \rho'_a \otimes \rho'_a \otimes \rho'_b \otimes \rho'_b$, where $|0\rangle$ is the control qubit, is subjected to the controlled unitary gate U. This modifies the interference of the controlled qubit by the factor $\mathrm{Tr}[\rho U] = v e^{i\alpha}$, with v and α being the visibility and phase shift of the interference fringes, respectively [316–319]. Two such schemes (corresponding to $\mathrm{Tr}[(\rho'_a)^2 (\rho'_b)^2]$ and $\mathrm{Tr}[(\rho'_a \rho'_b)^2]$) lead to the quantumness $\mathcal{M}(\rho'_a, \rho'_b) = 4(v_1 - v_2)$, where v_1 and v_2 correspond to the respective visibilities obtained by the action of relevant unitary gates. We motivate the present discussion by illustrating this notion on some of the channels discussed above.

(a) For RTN, the two visibilities (with $x = \phi = 0$) correspond to

$$
\mathrm{Tr}[(\rho'_a \rho'_b)^2] = \frac{1}{4}, \quad \mathrm{Tr}[(\rho'_a)^2 (\rho'_b)^2] = \frac{1}{4}(1 + [\Lambda(t)]^2).
\tag{4.96}
$$

Making use of these in Eq. (4.95), we obtain $\mathcal{M}(\rho'_a, \rho'_b) = [\Lambda(t)]^2$, consistent with the definition in Eq. (4.85), see below Eq. (4.92).

(b) For GDC, the two visibilities (with $x = \phi = 0$) turn out to be

$$
\begin{aligned}
\mathrm{Tr}[(\rho_a \rho'_b)^2] &= 1/4 - 2(-1 + p_1 + p_2)(p_1 + p_2)(-1 + p_2 + p_3)(p_2 + p_3), \\
\mathrm{Tr}[(\rho'_a)^2 (\rho'_b)^2] &= 1/2(1 + 2p_1^2 + 2(-1 + p_2)p_2 + p_1(-2 + 4p_2))(1 + 2p_2^2 \\
&\quad + 2(-1 + p_3)p_3 + p_2(-2 + 4p_3)).
\end{aligned}
\tag{4.97}
$$

These lead to the expression $\mu = \mathcal{M}(\rho'_a, \rho'_b)|_{\phi=0} = (p_0 + p_1 - p_2 - p_3)^2 (p_0 - p_1 - p_2 + p_3)^2$ in accord with the definition in Eq. (4.85), see Eq. (4.94).

What makes this approach particularly attractive is that here the quantumness of the channel can be experimentally determined.

4.8 Results and discussion

The quantumness of two arbitrary states ρ and σ can be identified with their incompatibility and quantified by $\mu = \max_{\rho, \sigma} \mathcal{M}(\rho, \sigma)$ as defined in Sec. (4.5.1). For a mixed initial diagonal state $\rho_0 = \sum_i \lambda_i |i\rangle\langle i|$, which evolves to ρ_t under some dynamics, the following inequality holds [288]

$$
\frac{\mathcal{M}(\rho_0, \rho_t)}{4} \le F(\rho_0, \rho_t) \le \frac{C_{l_1}(\rho_0, \rho_t)}{2}.
\tag{4.98}
$$

Table 4.2: Various quantum channels, introduced at the beginning of Sec. (4.6), with their Kraus operators and the quantumness using commutation based measure $\mu = \max_{\rho_a,\rho_b} \mathcal{M}(\rho_a', \rho_b')$. For the sake of comparision, the corresponding results based on the coherence based measure $Q_{C_{l_1}}$ [107] are also provided. Here, $\tilde{\xi} = \frac{5}{2}(\alpha - 1)^2(1 - \xi)^2$ and $\tau = \frac{-2}{\gamma(2n+1)} \ln\left[\frac{5}{6+4n+n^2}\right]$ [107].

Channel	Kraus operators	μ	$Q_{C_{l_1}}$
RTN	$K_0 = k_+ \begin{pmatrix} 1 & 0 \\ 0 & 1 \end{pmatrix}, K_1 = k_- \begin{pmatrix} 1 & 0 \\ 0 & -1 \end{pmatrix}.$	$[\Lambda(t)]^2$	$[\Lambda(t)]^2$
NMD	$N_0 = n_+ \begin{pmatrix} 1 & 0 \\ 0 & 1 \end{pmatrix}, N_1 = n_- \begin{pmatrix} 1 & 0 \\ 0 & -1 \end{pmatrix}.$	$[\Omega(p)]^2$	$[\Omega(p)]^2$
PD	$P_0 = \begin{pmatrix} 1 & 0 \\ 0 & \sqrt{1-\gamma} \end{pmatrix}, P_1 = \begin{pmatrix} 1 & 0 \\ 0 & \sqrt{\gamma} \end{pmatrix}.$	$1 - \gamma$	$1 - \gamma$
Unruh	$U_0 = \begin{pmatrix} \cos(r) & 0 \\ 0 & 1 \end{pmatrix}, U_1 = \begin{pmatrix} 0 & 0 \\ \sin(r) & 0 \end{pmatrix}.$	$\cos^2(r)$	$\cos^2(r)$
AD	$A_0 = \begin{pmatrix} 1 & 0 \\ 0 & \sqrt{1-\gamma} \end{pmatrix}, A_1 = \begin{pmatrix} 0 & \sqrt{\gamma} \\ 0 & 0 \end{pmatrix}$	$1 - \gamma$	$1 - \gamma\ (\gamma > \frac{1}{6})$ $\frac{1}{6}(6\gamma^2 - 3\gamma + 2)\ (\gamma \le \frac{1}{6})$
GAD	$G_0 = \begin{pmatrix} \sqrt{\alpha} & 0 \\ 0 & \sqrt{\alpha\xi} \end{pmatrix}, G_1 = \begin{pmatrix} 0 & \sqrt{\alpha P} \\ 0 & 0 \end{pmatrix}, G_3 = \begin{pmatrix} \sqrt{\beta\xi} & 0 \\ 0 & \sqrt{\beta} \end{pmatrix},$ $G_4 = \begin{pmatrix} 0 & 0 \\ \sqrt{\beta P} & 0 \end{pmatrix}.$	$\xi\left(\xi - \sqrt{2}(\xi - 1)\right)^2$ $(\xi > 1)$ $\xi(-1 + 2\xi)^2$ $(\xi < 1)$	$\xi^2\ (t > \tau)$ $\frac{1}{2}\xi + \tilde{\xi}\ (t \le \tau)$

Here, $F(\rho_0, \rho_t)$ is the quantum Fisher information and $C_{l_1}(\rho_0, \rho_t)$ is the l_1-norm coherence; both well known measures of quantumness. The commutator based measure provides a lower bound and a reliable witness of quantumness.

In this work, we extend the approach of quantifying the quantumness of states, in terms of their incompatibility, to explore the quantumness of channels. This method involves starting with two states which are maximally non-commuting and subjecting them to a quantum channel. The incompatibility of the resulting output states can be attributed to the degree of quantumness of the channel. We have computed the quantumness of various well known channels and compared them with the analogous estimation of quantumness from coherence based measure [298]. These are listed in Table (4.2). It is interesting to note that quantumness from the proposed measure is in good agreement with that with the coherence based measure [107]. This is consistent with our intuition as coherence is related to the off-diagonal elements of the density matrix as would be the cause for noncommutativity between the states. It should be noted that in the case of GDC, the coherence based measure leads to quantumness $(p_0 - p_1)^2 + (p_2 - p_3)^2$, different from that obtained by the commutation based measure adapted here. This is consistent with Eq. (4.98).

However, the attractive feature here is that the measure proposed can be calculated easily and is also amenable to experimental determination. Further, from the cases of the RTN and NMD channels, it is evident that quantumness reflects the non-Markovian nature of the channel under consideration.

4.9 Leggett Garg inequality under non-Markovian noise

In this section, which is based on [99], we study the effect of non-Markovianity on temporal correlations, in particular, as part of a test for LGI. That temporal correlations will also be affected by non-Markovianity, as are general quantum phenomena, is not surprising. Indeed, a sufficient but not necessary measure for non-Markovianity in terms of a temporal steerable weight is given in [320]. However, there is an important fact to be recognized here, which is that non-Markovianity in general involves setting up system-bath correlations, even through the system and bath may be initially uncorrelated. Therefore, the intervention of measurement that is done to produce temporal correlations, will in general re-prepare the environment also, just as it re-prepares the system. Hence, correlations based on a subsequent measurement will be subject, in general, to a different noisy channel than the first measurement.

From a quantum information theoretic perspective, non-Markovianity has of late been studied by the (not always equivalent) criteria of (CP) divisibility and distinguishability [101]. In particular, non-Markovianity according to the former criterion manifests as the fact that the *intermediate map* (i.e., the dynamical map that propagates an intermediate earlier state to a later state) acting on the density operator is not-completely-positive (NCP) [95]. As a result, the intermediate time evolution of the density operator is no longer given by the Kraus operator-sum representation. Instead, the operator sum-difference representation must be employed [102], wherein the trace-preserving NCP map is represented as the difference of two CP maps.

The failure of the quantum regression hypothesis (QRH) [103], which deals with multi-time correlation functions, also captures a traditional idea of quantum non-Markovianity [104]. In recent times, there have been a number of works that compute the two-time correlation functions for non-Markovian dynamics. For example, the evolution equations for the two-time correlation functions for non-Markovain evolution in the case of weak system-environment coupling was studied in [105], employing the full system-environment Hamiltonian. In particular, with regard to the question of the LGI violation in the context of non-Markovian noise, building on [105], the LGI violations for a two-level system under non-Markovian dephasing was studied in [321]. A similar problem for the Jaynes-Cummings model was discussed in [106]. The common theme in these works is to start from the full unitary evolution and then derive the evolution equations for the correlation functions using the appropriate limits.

As noted above, because under non-Markovianity, system measurements can disturb the bath, and hence care must be exercised in computing two-time correlations if the reduced dynamics alone is used. Here, we study LGI violation in the non-Markovian regime which, to our knowledge, is the first instance where this is done using the system's reduced dynamics. We argue that a purely reduced dynamics approach can be adopted, with the proviso that the noise is suitably updated after the first (and subsequent) intervention(s).

Here, we present a description of a simple non-Markovian model and its characterization. This is followed by investigation of LGI in the context of this model.

4.9.1 A simple model

Given times $t_2 > t_1 > t_0$ during the evolution of an open system, suppose a projective measurement is performed at time t_1. If the environment is (approximately) stationary during the interval $[t_0, t_2]$, then the same channel can be considered as acting in the intervals (t_1, t_2) and (t_0, t_1). Let the Hilbert spaces of the system and environment be denoted by $\mathcal{H}_S$ and $\mathcal{H}_E$, respectively; with initial states $|\psi_S\rangle \in \mathcal{H}_S$ and $|\psi_E\rangle \in \mathcal{H}_E$, respectively. The combined state $|\psi_S\rangle \otimes |\psi_E\rangle$ lives in the tensor product space $\mathcal{H}_S \otimes \mathcal{H}_E$. The total dynamics is given by unitary (U), and would in general entangle the system and environment degrees of freedom such that

the reduced dynamics, say from t_0 to t_1, is described by the Kraus operators $K_\mu(t_1 - t_0) = \langle e_\mu | U(t_1 - t_0) | \psi_E \rangle$, where $\{|e_\mu\rangle\}$ is a basis for the environment. An act of measurement at time t_1 would collapse the system in an eigenstate of the projector and simultaneously modify the state of environment to $|\psi'_E\rangle$. The new Kraus operators, governing the dynamics from t_1 to t_2 would be $K'_\mu(t_2 - t_1) = \langle f_\mu | U(t_2 - t_1) | \psi'_E \rangle$, where $|f_\mu\rangle = e^{i\xi} |e_\mu\rangle$ is a new environment basis. Assuming that the environment state changes only by a global phase $e^{i\chi}$, i.e., $|\psi'_E\rangle = e^{i\chi} |\psi_E\rangle$, we have $K'_\mu(t_2 - t_1) = e^{i(\xi-\chi)} K_\mu(t_1 - t_0)$. Thus the two Kraus operators differ only by a global phase factor and hence describe the same dynamics, i.e., the reduced dynamics they produce has the same time dependence.

Here, a crucial assumption made was that the act of measurement changes the state of environment at most by a global phase. We will now illustrate, using a simple model, that such an assumption does not hold for non-Markovian dynamics and one needs to update the post measurement map depending upon the measurement outcome. If the system dynamics is indivisible, then the system-bath interaction would generate entanglement. Clearly, the above argument will no longer hold, requiring the system dynamics to be modified post-measurement. To see how one must modify it, we consider a simple model of system-bath interaction.

Consider a single qubit system interacting with a single qubit environment with the initial states given by

$$|\psi_S\rangle = (|0_S\rangle + |1_S\rangle)/\sqrt{2} \qquad \text{and} \qquad |\psi_E\rangle = (|0_E\rangle + |1_E\rangle)/\sqrt{2}, \tag{4.99}$$

where the subscripts S and E correspond to system and environment, respectively. Let us assume a separable state at time $t = 0$, that is, $|\psi(0)\rangle = |\psi_S\rangle \otimes |\psi_E\rangle$. We adopt the Jaynes-Cummings type Hamiltonian (with $\hbar = 1$)

$$H = \omega \Big(|01\rangle\langle 10| + |10\rangle\langle 01| \Big), \tag{4.100}$$

such that the time evolution is generated by unitary operator $U(t) = e^{-iHt}$ and the state at some later time t is given by $|\psi(t)\rangle = U(t) |\psi(0)\rangle$. Let us define the density matrices corresponding to system $\rho_S = |\psi_S\rangle \langle \psi_S|$, environment $\rho_E = |\psi_E\rangle \langle \psi_E|$, and the composite state $\rho_{SE}(t) = |\psi(t)\rangle \langle \psi(t)|$.

Characterization of non-Markovian dynamics: Here, we investigate the non-Markovian features of the above mentioned model by studying Sudarshan's $\boldsymbol{A}$ and $\boldsymbol{B}$ dynamical maps [222]. The map $\boldsymbol{A}$ is constructed by vectorizing the reduced system density matrix $\boldsymbol{\rho}_S$, obtained by tracing over the environment E, such that $\boldsymbol{\rho}'_S = \boldsymbol{A}.\boldsymbol{\rho}_S$, or $\boldsymbol{\rho}_{p,q}(t_0) \rightarrow \boldsymbol{\rho}'_{p,q}(t) = \boldsymbol{A}_{pq;rs}(t,t_0)\boldsymbol{\rho}_{r,s}(t_0)$.

$$\boldsymbol{A}(t,0) = \begin{pmatrix} \frac{1}{4}(\cos(2t\omega) + 3) & \frac{1}{4}i\sin(2t\omega) & -\frac{1}{2}i\sin(t\omega) & \cos(t\omega) \\ \frac{1}{2}i\sin(t\omega) & \cos(t\omega) & 0 & -\frac{1}{2}i\sin(t\omega) \\ -\frac{1}{2}i\sin(t\omega) & 0 & \cos(t\omega) & \frac{1}{2}i\sin(t\omega) \\ \frac{1}{2}\sin^2(t\omega) & -\frac{1}{4}i\sin(2t\omega) & \frac{1}{4}i\sin(2t\omega) & \frac{1}{4}(\cos(2t\omega) + 3) \end{pmatrix}. \tag{4.101}$$

In order to show the CP indivisibility of the map, we divide the time evolution between $(0, t)$ into interval $(0, t/2)$ and $(t/2, t)$, such that $\boldsymbol{A}(t, t/2) = \boldsymbol{A}(t, 0)\boldsymbol{A}^{-1}(t/2, 0)$. One can then construct the $\boldsymbol{B}(t, t/2)$ map, which is basically the Choi matrix, by using

$$\boldsymbol{B}_{pr;qs}(t, t/2) = \boldsymbol{A}_{pq;rs}(t, t/2). \tag{4.102}$$

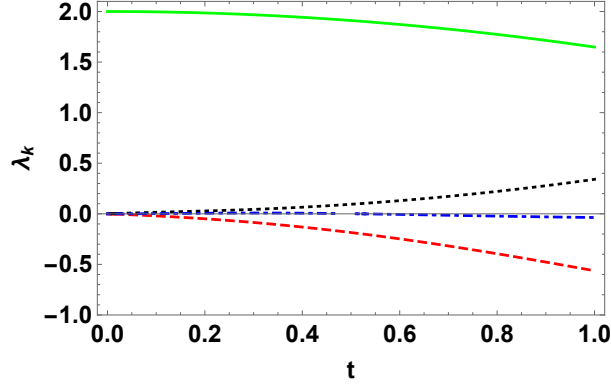The eigenvalues of this matrix are plotted in Fig. 4.20

Figure 4.20: Eigenvalues λ_k ($k = 1, 2, 3, 4$) of the Choi matrix $B_{pr;qs}(t, t/2)$. Negative eigenvalues indicate that the map is NCP.
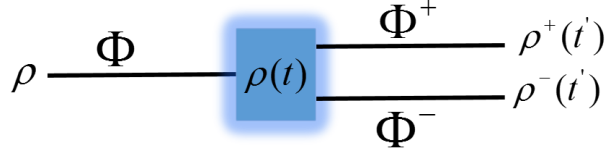

Figure 4.21: A measurement of a dichotomic observable on $\rho(t)$ would be followed by two possible dynamics depending on its outcome. The map Φ (Eq. (4.105)) would be replaced by Φ^+ and Φ^- (Eq. (4.112)) depending on whether the outcome is $+1$ or -1, respectively.

In order to verify that the map is P-indivisible, it is enough to show that the evolution under this map leads to increase in the distinguishability of two states. This can be shown by looking at the behavior of trace distance function between two orthogonal states subjected to the map Φ described by Eq. (4.105) below, obtained from the Choi matrix Eq. (4.101). Consider two orthogonal states $\rho_0(0) = |0\rangle \langle 0|$ and $\rho_1(0) = |1\rangle \langle 1|$, evolved under this map to $\rho_0(t) = \Phi[\rho_0(0)]$ and $\rho_1(t) = \Phi[\rho_1(0)]$, respectively.

The trace distance between these states is defined as $\mathrm{TD} = \frac{1}{2} \sum_k |\eta_k|$, where η_k are the eigenvalues of matrix $\rho_0(t) - \rho_1(t)$. We have

$$\mathrm{TD} = \sqrt{\frac{7 + \cos(\omega t)}{2}}. \tag{4.103}$$

It is clear that TD is an oscillating function of time. The recurrent behavior of TD is a signature of P-indivisibility of the map.

Reduced dynamics: The reduced state of the system can be obtained by tracing over the environment. Denoting the set of basis states of the environment as $\{|e_\mu\rangle\}$, we have $\rho_S(t) = \sum_\mu \mathcal{K}_\mu \rho_S \mathcal{K}_\mu^\dagger$, where $\mathcal{K}_\mu = \langle e_\mu | U(t) | \psi_E \rangle$ are the Kraus operators. With the Hamiltonian given by Eq. (4.100) and the environment state given in Eq. (4.99) (the environment basis states $\{|e_\mu\rangle = |0_E\rangle, |1_E\rangle\}$), we obtain

$$\mathcal{K}_0 = \begin{pmatrix} \frac{1}{\sqrt{2}} & 0 \\ -\frac{i \sin(\omega t)}{\sqrt{2}} & \frac{\cos(\omega t)}{\sqrt{2}} \end{pmatrix}, \quad \text{and} \quad \mathcal{K}_1 = \begin{pmatrix} \frac{\cos(\omega t)}{\sqrt{2}} & -\frac{i \sin(\omega t)}{\sqrt{2}} \\ 0 & \frac{1}{\sqrt{2}} \end{pmatrix}, \tag{4.104}$$

71

satisfying the completeness relation $\mathcal{K}_0^\dagger \mathcal{K}_0 + \mathcal{K}_1^\dagger \mathcal{K}_1 = \mathbf{1}$.

$$\Phi[\rho_S(0)] = \sum_\mu \mathcal{K}_\mu \rho_S(0) \mathcal{K}_\mu^\dagger. \tag{4.105}$$

It is possible to show that the same map can be constructed by directly obtaining the Kraus operators from the Choi matrix corresponding to map A given in Eq. (4.101).

Let us define the projectors on the system space as $\Pi^+ = |0_S\rangle\langle 0_S| \otimes \mathbf{1}_E$ and $\Pi^- = |1_S\rangle\langle 1_S| \otimes \mathbf{1}_E$. Here, $\mathbf{1}_E$ is the identity operator on the environment Hilbert space. Applying these projectors on time evolved state of the combined system, the (normalized) post measurement states in the two cases are given respectively as:

$$|\phi^o(t)\rangle = \frac{1}{\sqrt{2}} \begin{pmatrix} 1 \\ e^{-i\omega t} \\ 0 \\ 0 \end{pmatrix} = \begin{pmatrix} 1 \\ 0 \end{pmatrix} \otimes \frac{1}{\sqrt{2}} \begin{pmatrix} 1 \\ e^{-i\omega t} \end{pmatrix}, \tag{4.106}$$

$$|\phi^1(t)\rangle = \frac{1}{\sqrt{2}} \begin{pmatrix} 0 \\ 0 \\ e^{-i\omega t} \\ 1 \end{pmatrix} = \underbrace{\begin{pmatrix} 0 \\ 1 \end{pmatrix}}_{system} \otimes \underbrace{\frac{1}{\sqrt{2}} \begin{pmatrix} e^{-i\omega t} \\ 1 \end{pmatrix}}_{environment}. \tag{4.107}$$

Therefore we have two possible evolutions with the following system and environment states

$$|\chi_S(0)\rangle = |0\rangle, \qquad |\chi_E(0)\rangle = \frac{|0\rangle + e^{-i\omega t}|1\rangle}{\sqrt{2}}, \qquad post\ \Pi^+\ measurement \tag{4.108}$$

and

$$|\chi_S(0)\rangle = |1\rangle, \qquad |\chi_E(0)\rangle = \frac{e^{-i\omega t}|0\rangle + |1\rangle}{\sqrt{2}}, \qquad post\ \Pi^-\ measurement. \tag{4.109}$$

The corresponding Kraus operators turn out to be

$$\mathcal{K}_0^+(t) = \begin{pmatrix} \frac{1}{\sqrt{2}} & 0 \\ -\frac{ie^{-i\omega t}\sin(\omega t)}{\sqrt{2}} & \frac{\cos(\omega t)}{\sqrt{2}} \end{pmatrix}, \qquad \mathcal{K}_1^+(t) = \begin{pmatrix} \frac{e^{-i\omega t}\cos(\omega t)}{\sqrt{2}} & -\frac{i\sin(\omega t)}{\sqrt{2}} \\ 0 & \frac{e^{-i\omega t}}{\sqrt{2}} \end{pmatrix}, \tag{4.110}$$

and

$$\mathcal{K}_0^-(t) = \begin{pmatrix} \frac{e^{-i\omega t}}{\sqrt{2}} & 0 \\ -\frac{i\sin(\omega t)}{\sqrt{2}} & \frac{e^{-i\omega t}\cos(\omega t)}{\sqrt{2}} \end{pmatrix}, \qquad \mathcal{K}_1^-(t) = \begin{pmatrix} \frac{\cos(\omega t)}{\sqrt{2}} & -\frac{ie^{-i\omega t}\sin(\omega t)}{\sqrt{2}} \\ 0 & \frac{1}{\sqrt{2}} \end{pmatrix}. \tag{4.111}$$

We denote the corresponding maps by $\Phi^\pm$

$$\Phi^\pm[\rho(0)] = \sum_\mu \mathcal{K}_\mu^\pm \rho(0) (\mathcal{K}_\mu^\pm)^\dagger \tag{4.112}$$

Figure 4.21 summarizes the various steps discussed above.

4.9.2 Leggett-Garg inequality

Here, we study the violation of the LGI in the above discussed model. The three time LG parameter is given by

$$K_3 = C(0,t) + C(t,2t) - C(0,2t), \tag{4.113}$$

where $C(t_i, t_j) = p(^+t_i)q(^+t_j|^+t_i) - p(^+t_i)q(^-t_j|^+t_i) - p(^-t_i)q(^+t_j|^-t_i) + p(^-t_i)q(^-t_j|^-t_i)$, with

$$p(^a t_i)q(^b t_j|^a t_i) = \text{Tr}\left\{\Pi^b \sum_{\nu,\mu} \tilde{K}_\nu(t_j - t_i)\Pi^a K_\mu(t_i)\rho(0)K_\mu^\dagger(t_i)\Pi^a \tilde{K}_\nu^\dagger(t_j - t_i)\right\}.$$

Here, $\tilde{K}_\nu$ is the post measurement Kraus operator $\mathcal{K}_{0,1}^\pm$, given by Eqs. (4.110) and (4.111), which in general, will be different from K_μ. With a general dichotomic operator

$$O = \begin{pmatrix} \cos(\theta) & e^{i\phi}\sin(\theta) \\ e^{-i\phi}\sin(\theta) & -\cos(\theta) \end{pmatrix}. \tag{4.114}$$

parametrized by $-\pi \leq \theta < \pi$; $\pi/2 \leq \phi \leq \pi/2$ [322], and the general qubit state $|\psi(0)\rangle = \cos(\theta_s/2)|0\rangle + e^{i\phi_s}\sin(\theta_s/2)$, with $0 \leq \theta \leq \pi$; $0 \leq \phi < 2\pi$, the explicit expressions of the two time correlation functions turn out to be

$$\begin{aligned}
C(0,t) &= -8\sin(\theta)\cos(\theta)\cos(\phi)\sin^4\left(\frac{\omega t}{2}\right)\cos^2\left(\frac{\omega t}{2}\right)(\sin(\theta)\sin(\theta_s)\cos(\phi + \phi_s) \\
&\quad + \cos(\theta)\cos(\theta_s)) + \cos(\omega t)\left(\sin^2(\theta) + \cos^2(\theta)\cos(\omega t)\right) \\
&\quad - \frac{1}{4}\sin(2\theta)\sin(\phi)\sin(2\omega t)(\cos(\omega t) - 1),
\end{aligned}$$

$$\begin{aligned}
C(t,2t) &= \frac{1}{2}\cos(\omega t)[1 + \sin(\theta)] + \frac{\cos(\omega t)\cos(\theta)}{2}T_1 - \frac{1}{4}\sin(2\theta)\cos(\phi)\sin^3(\omega t)\sin^2(\frac{\omega t}{2})T_2 \\
&\quad - \frac{(-1 + \cos(\omega t))}{4}\sin(2\theta)\sin(\phi)\sin(2\omega t). \tag{4.115}
\end{aligned}$$

where

$$\begin{aligned}
T_1 &= \cos(\theta)(2\cos(\omega t) - 1) - 16\sin(\theta)\cos(\phi)\sin^4\left(\frac{\omega t}{2}\right)\cos^2\left(\frac{\omega t}{2}\right) \\
&\quad \times (\sin(\theta)\sin(\theta_s)\cos(\phi + \phi_s) + \cos(\theta)\cos(\theta_s)\cos(\omega t)), \\
T_2 &= \sin(\theta)\cos(\theta_s)\sin(\phi) + \cos(\theta)\sin(\theta_s)\sin(\phi_s)\cos(\omega t). \tag{4.116}
\end{aligned}$$

Note that (θ_s, ϕ_s) and (θ, ϕ) are the state and measurement variables, respectively. For $\theta = \pi/2$, the expressions simplify to $C(0,t) = C(t,2t) = \cos(\omega t)$; consequently $K_3 = 2\cos(\omega t) - \cos(2\omega t)$. Figure 4.22 depicts the violations of the LGI for various state and measurement settings. Thus for example, from the perspective of LGI violations, we see that given fixed measurement settings, some state preparations are preferable over the others. Also, with fixed state preparation, some measurements are more favorable for the purpose.
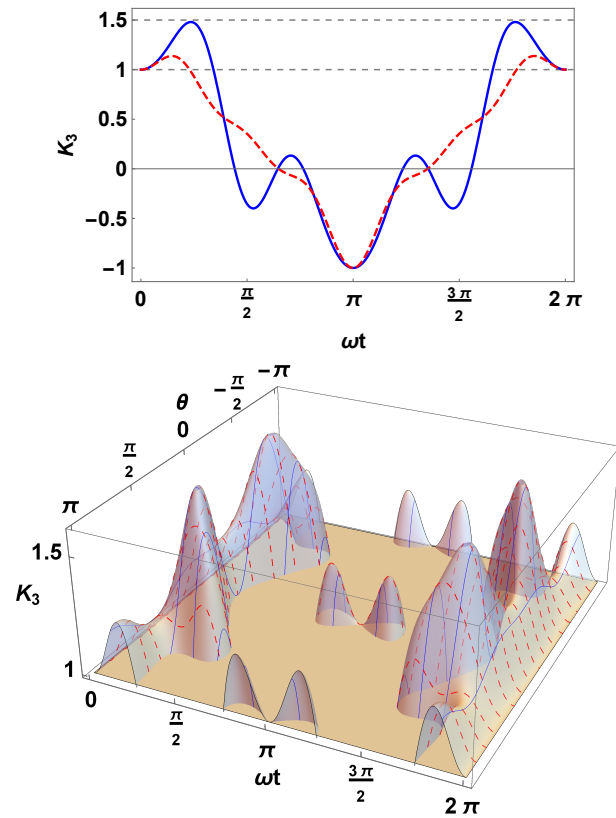
Figure 4.22: Left: Leggett-Garg parameter as defined in Eq. (4.113), with correlation functions given by Eq. (4.115) . Solid (blue) and dashed (red) curves correspond to the state variables $\theta_s = \pi/2$, $\phi_s = 0$ and $\theta_s = \pi$, $\phi_s = 0$, respectively. The measurement parameters used are $\theta = \pi/4$, $\phi = 0$. The right plot shows the variation of K_3 with respect to time as well as the measurement variable θ (with $\phi = 0$). The state variables used in this case are $\theta_s = \pi/2$, $\phi_s = 0$.

4.10 Conclusion

In Sec. 4.2, we considered two quantum channels namely Random Telegraph Noise (RTN) and non-Markovian dephasing (NMD) and studied the dynamics of a general qubit state in these models. The dynamics is governed by completely positive and trace preserving Kraus operators. The quantum Fisher information flow, which has recently been proposed as a witness of the non-Markovian behavior, is analyzed and is found consistent with the analysis made using the decoherence rates in these models. Further, various facets of quantum information viz., quantum coherence, mixedness, average gate fidelity and channel fidelity are studied, their compact analytical expressions are obtained and their behavior is contrasted in the Markovian and non-Markovian regimes for the RTN channel. Even though both RTN and NMD show non-Markovian behavior, there is a distinction between the two. The non-Markovian dynamics for the RTN model has a characteristic recurrent behavior, not found in the case of NMD. Nevertheless, a symmetric trade-off between coherence and mixedness, quantified by a coherence-mixedness balance parameter β, is observed in both the cases, thereby testifying to their basic dephasing nature. Such characterization of the quantum channels can be significant from the perspective of carrying out quantum information and communication tasks.

Section 4.3 was devoted to study the violation of Leggett-Garg type inequalities in a driven two level atom interacting with a squeezed thermal bath. The effect of various experimentally relevant parameters on the violation of the inequality were examined carefully. The violations were seen to be prominent in the underdamped case. The increase in temperature was found to decrease the degree of violation as well as the time over which the violation is sustained. Squeezing the thermal state of the reservoir was also found to reduce the violation of LGtIs. Enhanced violations, reaching to the quantum bound, were witnessed in the strong driving limit. Further, we studied the effect of the weak measurements on the extent of violation of LGtI. The weak measurements are characterized by the parameter ξ such that $\xi = 0$ ($\xi = 1$) corresponds to no measurement (ideal projective measurement). The maximum violation was found to occur for the ideal projective measurements. This study therefore highlights the role of various external parameters on the quantumness of the system.

We studied, in Sec. 4.4, the quantumness and average fidelity of various channels, both Markovian as well as non-Markovian. Specifically, we considered the dephasing channels like RTN, NMD and PD channels and non-dephasing channels such as GAD and Unruh channels. The non-Markovian dynamics (exhibited by RTN and NMD channels in this case) is found to favor the nonclassicality. This is explicitly seen from the fact that a nonzero value of parameters controlling the degree of non-Markovianity takes the quantumness beyond the classical value. The non-Markovianity assisted enhancement of nonclassicality can be of profound importance in carrying out quantum information tasks. This can be realized by effectively engineering the system-reservoir models. The quantumness measure and average fidelity exhibit similar predictions for the Unruh channel. Similar behavior is observed for the dephasing channels, albeit, in the Markovian regime. This can bee seen in RTN and NMD channels. In contrast, in the non-dephasing Lindbladian channel, considered here, the quantumness witness and average fidelity show qualitatively similar results. Such a study of the interplay between nonclassicality of the quantum channels with the underlying dynamics can be useful from the quantum information point of view, and also brings out the effectiveness of the measure of quantumness under different types of dynamics.

In Sec. 4.5, we proposed a measure to quantify the degree of quantumness of a channel. The quantum channels provide a way to describe the processes where pure states go over to the mixed ones. Therefore, it is natural to ask how well a quantum channel preserves the quantumness

of the states which are subjected to it. Recently, a measure based on the l_1-norm coherence was introduced to quantify the quantumness of channels. We have addressed the problem by using an intuitive approach based on the incompatibility of the states. The quantumness of a system is identified with the mutual non-commutation of all its accessible states. We illustrated the approach developed here by considering various examples of quantum channels, both Markovian as well as non-Markovian, and found that our results are in good agreement with the coherence based measure. An added attraction of this method is that it can be probed experimentally.

The violation of the LGI under non-Markovian evolution has been studied in Sec. 4.9 by using the reduced dynamics. Difficulties in handling the two time correlation functions under non-Markovian evolution were highlighted and a possible way of handling them was illustrated by a simple model. The non-Markovian nature of the model was characterized by negative eigenvalues of the Choi matrix implying CP-indivisibility. The increase in the trace distance function with time brought out the P-indivisibility of the map. The non-Markovian dynamics involves setting up of system-bath correlations; and measurements disrupt these correlations. Therefore, a full system-bath Hamiltonian approach is natural. However, we have pointed out how the problem can be dealt with from a reduced dynamics perspective. The key point is that the noise superoperator acting on the system must be suitably updated after a measurement intervention.